Climate of Eastern Africa

Pierre Camberlin

Climate of Eastern Africa

Pierre Camberlin

Summary

Eastern Africa, classically presented as a major dry climate anomaly region in the otherwise wet equatorial belt, is a transition zone between the monsoon domains of West Africa and the Indian Ocean. Its complex terrain, unequaled in the rest of Africa, results in a huge diversity of climatic conditions that steer a wide range of vegetation landscapes, biodiversity and human occupations. Meridional rainfall gradients dominate in the west along the Nile valley and its surroundings, where a single boreal summer peak is mostly observed. Bimodal regimes (generally peaking in April and November) prevail in the east, gradually shifting to a single austral summer peak to the south. The swift seasonal shift of the Intertropical Convergence Zone and its replacement in January-February and June-September by strong meridional, generally diverging low-level winds (e.g., the Somali Jet), account for the low rainfall. These large-scale flows interact with topography and lakes, which have their own local circulation in the form of mountain and lake breezes. This results in complex rainfall patterns, with a strong diurnal component, and a frequent asymmetry in the rainfall distribution with respect to the major relief features. Whereas highly organized rain-producing systems are uncommon, convection is partly modulated at intra-seasonal (about 30-60-day) timescales. Interannual variability shows a fair level of spatial coherence in the region, at least in July-September in the west (Ethiopia and Nile Valley) and October-December in the east along the Indian Ocean. This is associated with a strong forcing from sea-surface temperatures in the Pacific and Indian Oceans, and to a lesser extent the Atlantic Ocean. As a result, Eastern Africa shows some of the largest interannual rainfall variations in the world. Some decadal-scale variations are also found, including a drying trend of the March-May rainy season since the 1980s in the eastern part of the region. Eastern Africa overall mean temperature increased by 0.7 to 1°C from 1973 to 2013, depending on the season. The strong, sometimes non-linear altitudinal gradients of temperature and moisture regimes, also contribute to the climate diversity of Eastern Africa.

Keywords: Eastern Africa, rainfall regimes, highland climates, atmospheric circulation, climate variability

To Gérard Beltrando and Raphael Okoola, who contributed to our knowledge of East African climates and both left us too soon in early 2016.

Eastern Africa, also called the Greater Horn of Africa, covers eleven countries (Sudan, South Sudan, Eritrea, Djibouti, Ethiopia, Somalia, Kenya, Uganda, Rwanda, Burundi, Tanzania). In the tropical belt, Eastern Africa stands out as a relatively dry area, despite its equatorial location. Between 12°S and 12°N, it is actually the driest land area (Yang et al., 2015). Trewartha (1961) emphasized the "widespread deficiency of rainfall" in the region as "the most impressive climatic anomaly in all of Africa".

This region is characterized by low average incomes: all the 11 countries belong to the 25% poorest nations in the world, based on per capita gross domestic product (GDP) at purchasing power parity (World Bank, 2014). This fact, added to the dependence of national economies to the agricultural sector, in terms of GDP and employment, makes climatic conditions and particularly rainfall a crucial issue for social and economic development.

1. Geographical features influencing the region's climate

Eastern Africa encloses both the highest and the lowest points of the African continent. This wide altitudinal range, from Lake Assal in Djibouti (153 m below mean sea-level) to Mount Kilimanjaro in Tanzania (5895 m above mean sea-level), is emblematic of a region of strong elevation gradients and highly diverse topographical environments.

The highlands form an almost continuous north-south barrier from the Red Sea to southern Tanzania (fig.1). They include the Ethiopian Massif, the most extensive highland area in Africa, with almost 50% of the continent's areas above 1500 m (McCann, 1995). Large tablelands are dissected by deep valleys, and dominated by several summits culminating above 4000 m. Further south lie the East African Highlands *per se*, organized as two mountain arcs following the eastern and the western Rift valleys, from about 4°N to 10°S. In the east, the Kenya Highlands, at an average elevation of 1500-2500m, are flanked to the east and south-east by Africa's two highest mountains: Mt Kenya (5199 m) and Mt Kilimanjaro (5895 m). To the south, they are prolonged by the Eastern Arc Mountains, of lower elevation. In the west, the western Rift Mountains run from western Uganda to southern Tanzania, and include several peaks above 3000 m, among which are the Rwenzori Mountains (5109 m). Between the two

arcs is a large tableland around 1000-1200 m, in which lies Lake Victoria. Overall, the East African Highlands have a major impact on both the regional and extra-regional climate (Slingo et al., 2005). In particular, the wet conditions prevailing over the Congo Basin are a result of the presence of the East African highlands. The local effect of relief on winds, temperature and rainfall is discussed in sections 3 to 6.

The north-south highland barrier is interrupted by a major gap, the Turkana gap, between the Ethiopian and the Kenya Highlands (fig.1). It is a 300-km wide depression, lower than 700 meters except for some isolated mountains. This gap, of great climatic significance (section 3), connects two major low-lying areas. The first one, to the northwest, corresponds to the Nile Plains, west of the Ethiopian Highlands, covering most of Sudan and South Sudan at an altitude between 300 and 500 meters. The second one, to the east, are the plains and low plateaus bordering the Indian Ocean, from Tanzania to eastern Kenya, eastern Ethiopia and Somalia. The coast itself is generally low. North of a west-east ridge which prolongs the Ethiopian Highlands, the Gulf of Aden trench connects to that of the Red Sea. Both constitute deep troughs bordered on the African and Arabian sides by major escarpments which act to channel the low-level winds. These troughs include a continental part, the Afar (or Danakil) depression, between Djibouti, eastern Eritrea and northeastern Ethiopia.

Eastern Africa exhibits a number of large waterbodies and extensive wetlands. Numerous elongated lakes dot the East African Rift system, from the Afar depression to Malawi (fig.1). The largest of these lakes are Lake Abbe and Lake Abaya, in the Ethiopian Rift Valley, Lake Turkana (6400 km^2), Lake Natron and Lake Eyasi in the eastern Rift, Lake Albert (5300 km^2), Lake Edward, Lake Kivu, Lake Tanganyika (32900 km^2) and Lake Rukwa, in the Western Rift, and finally Lake Malawi (or Nyassa, 29600 km^2) to the south. Several shallower lakes and swamps also occupy the basin between the Eastern Rift and the Western Rift, among which is Lake Victoria (68800 km^2), the second largest freshwater lake in the world. The African Great Lakes are important regulators for the regional climate (Thiery et al., 2015). In particular, Lake Victoria drives land-lake breezes which explain a strong late night maximum in convective activity over the lake (section 6). In South Sudan lie major swamp areas, among which the Sudd along the While Nile, whose area varies between 6700 and over 30000 km^2 depending on the season and year, and at an average of 20400 km^2 for 2001-2005 (Sutcliffe and Parks, 1999; Shamseddin et al., 2006). An average 7800 km^2 should be added for the Bahr-El-Ghazal

swamps, a tributary of the While Nile (Sutcliffe and Parks, 1999). South Sudan swamps have a strong effect, although mainly local, on temperature and rainfall (Zaroug et al., 2013).

Natural vegetation is dominated by (often wooded) grassland and shrubland. Over eastern Ethiopia, northern Somalia and northern Kenya, drier conditions result in open grassland and shrubland. The only continuous zones of closed evergreen forests lie in southwestern Ethiopia and on the edges of the Congo Basin (fig.1). Other isolated patches are found across parts of Kenya, Tanzania and Uganda, often on steep slopes. Being located in wet areas, they have been heavily encroached, although the resulting landcover is often an agroforest which includes many perennial species. Bare soil or bare rock dominate the shores of the Red Sea and Gulf of Aden, the Afar depression, parts of northern Somalia, the Turkana gap and the northern Sudan, where sandy areas are also found.

Cultivated areas are rapidly expanding, with a 28% increase between 1990 and 2010 in the region (Tanzania excluded; Brink et al., 2014). Landuse conversion to agriculture in Kenya, based on simulations with the RegCM4 regional climate model, was shown to drive a modest reduction in precipitation and a surface temperature increase in the Lake Victoria region (Otieno and Anyah, 2012). Irrigation remains limited in Eastern Africa. Among the main exceptions is the 8800 km^2 Gezira irrigation scheme in Sudan. Davenport and Hudson (1967) found that mean temperature, vapour pressure deficit and wind run were lower at the leeward edges of a 17-km transect across the Gezira cotton fields, resulting in much smaller evaporation than on the windward edge.Alter et al. (2015), based on observations and numerical experiments, found that the Gezira scheme locally inhibited rainfall while enhancing it to the east. The local rainfall inhibition results from decreased air temperature causing atmospheric subsidence, while there is increased upward motion to the east. Cloud development around Khartoum, Sudan was also found to be influenced by water surfaces (Hammer, 1970).

Other land use changes in Eastern Africa include the expansion of urban areas. Although Eastern Africa remains dominantly rural (in 2013 only Djibouti and Somalia had over 33% of urban population), capital cities are quickly spreading. The evidence of an urban heat island in Nairobi (Kenya), with an estimated population of 3.9 million in 2015 (United Nations, 2015) has been shown by Okoola (1980) and Makokha and Shisanya (2010). In Khartoum, Sudan, whose settled area increased fourfold between 1972 and 2000, and has an estimated 2015 population of 5.1 million, Elagib (2011) found a nocturnal urban warming, intensifying at

significant rates (1941-2005) with respect to the nearby rural station, for the dry and hot seasons. At daytime, the urban station is only marginally warmer and shows less warming over time than the rural station.

2. General atmospheric circulation features

Being located near the equator, Eastern Africa is directly affected by seasonal changes in the Hadley circulation, which implies a twice-a-year migration of the Intertropical Tropical Convergence Zone (ITCZ) across the region from south to north and backwards from north to south (Hills, 1979; Asnani, 1993; Nicholson, 1996). This migration is accompanied by a shift in the wind direction, from a northerly direction in boreal winter to a southerly direction in boreal summer, which is characteristic of the monsoons. Eastern Africa is located at the interface between two monsoon systems: the African monsoon to the west and the Indian Ocean monsoon to the east. The East African highlands are actually a major north-south barrier which both separates and connects the two systems. While the seasonal north-south amplitude of the African monsoon is limited, that of the Indian Ocean, from 15°S to 25°N, is the greatest in the world. This has major consequences on the climates of Eastern Africa.

In January (fig.2) and February, much of Eastern Africa is under the influence of low-level northeasterly winds from Egypt and the Arabian Sea. They are relatively dry (850 hPa specific humidity below 8 $g.kg^{-1}$) and divergent, especially over Somalia and Kenya, resulting in a stable atmosphere (Yang et al., 2015). The northeasterlies from the Arabian Sea are deflected by the Ethiopian and Kenya Highlands to enter the southern Red Sea and the Turkana gap as southeasterly air flows. A low-level jet actually develops over the Lake Turkana area as a result of orographic channeling (Kinuthia and Asnani, 1982; Nicholson, 2015a; see below). In the central Red Sea around 16-20°N, a surface confluence is found between the northerly and southerly flows, known as the Red Sea Convergence Zone (RSCZ) (Flohn, 1965b; Pedgley, 1966). A broad, diagonal ITCZ lies south of the study region, between the Congo Basin and southern Tanzania.

Three-dimensional atmospheric dynamics are shown through meridional cross-sections (fig.3). At 32°E, the northern Hadley cell is evident, with surface northerlies across the Nile plains, weak (near the equator) and moderate (near 10°S) rising motion further south, close to the ITCZ, and upper tropospheric southerlies. These southerly winds take a weak easterly

component in the southern hemisphere (Tropical Easterly Jet) and a strong westerly component in the northern hemisphere (Subtropical Westerly Jet). Subsidence is found north of 5-10°N, denoting the descending limb of the Hadley cell. At 37°E and 42°E the general pattern is the same, but the Hadley cell expands further south, as a result of the Indian winter monsoon penetrating far to the southern hemisphere. At 42°E mid-tropospheric descending motion is found to about 7°S. Relief has a significant effect at these longitudes. Upward motion is found on windward slopes or elevated surfaces (e.g., the Ethiopian Highlands), but north of the equator it is restricted to the lower troposphere, denoting shallow / dry convection.

By March, the dry northeasterlies from the northern Indian Ocean begin receding. In April (fig.2), over most of the region except Sudan, they are replaced by generally weak southeasterlies. The ITCZ moves over equatorial Eastern Africa, but contrary to West Africa it is diffuse, with no clear confluence of airflows from the two hemispheres. A mean low-level wind divergence is actually still found over the eastern plains from Somalia to eastern Kenya, and is particularly strong near the entrance of the Turkana Jet. The Indian Ocean being warmer, the southeasterlies bring over Eastern Africa a moister air mass than in January-February, especially towards the Lake Victoria basin and the slopes of the Ethiopian Highlands. But even in the middle of this season, there is net upper tropospheric convergence over Eastern Africa, as well as mean mid-tropospheric downward motion (or weak ascent only), conditions which are not highly propitious to rainfall (Yang et al., 2015). Over Sudan, the dry northeasterlies remain quite strong, but in the south appear wetter southwesterlies from the Congo Basin, in conjunction with a northward shift of the ITCZ to 10°N (fig.2).

During May, as a high pressure ridge builds up from the south and pressure decreases over the northern Indian Ocean, southeasterlies strengthen south of the equator and recurve to form southwesterlies in the opposite hemisphere over Somalia (not shown). This nascent monsoon flow is strongly divergent all along the East African plains bordering the Indian Ocean. It strengthens in June to form a low-level jet, the Somali jet. The transition from the boreal spring to the summer conditions is not always smooth but often characterized by two abrupt circulation changes in early April and late May, with corresponding jumps in the monsoon rain belt (Riddle and Cook, 2008; Riddle and Wilks, 2013). Discovered by Findlater (1969), the Somali jet is a western boundary current resulting from the pressure gradient between the Indian low and the Mascarene high (Anderson, 1976; Krishnamurti and Bhalme, 1976). With mean speeds of 10-15 $m.s^{-1}$ near 850 hPa in July-August (fig.2), the jet persists until September. The presence of

the East African Highlands intensifies the cross-equatorial flow and controls its vertical structure (Peagle and Geisler, 1986; Slingo et al. 2005; Chakraborty et al., 2009). The strong southerly flow brings in relatively dry and cool air from the southern hemisphere, resulting in atmospheric stability in most of Tanzania, eastern Kenya, Somalia and eastern Ethiopia (Yang et al., 2015). It cools the surface water in the Western Indian Ocean, causing further stability. Alongshore winds generate coastal upwelling in northeastern Somalia north of Obbia. Further west in the Nile Valley, the ITCZ gradually shifts from about 10°N in April to 17°N in July (fig.2; Osman and Hastenrath, 1969). The shift is accompanied by a replacement of the dry northeasterlies by moister southwesterlies, which are part of the African monsoon, but with moisture coming from both the Congo Basin and the Indian Ocean. A secondary, north-south convergence zone, the Congo Air Boundary (CAB), between the stable south-easterlies across Tanzania and the weak, moist westerlies shows well in the wind field and moisture contents, from the north of Lake Tanganyika to South Sudan. A minor convergence zone is also found in northern Uganda towards the western Kenya Highlands (fig.2; Anyamba and Kiangi 1985).

Meridional cross-sections for July (fig.3) show deep convection over the southern parts of the Nile Plains (32°E) and the Ethiopian Highlands (37°E), where ascending motion is very strong. Weaker ascent is found over the Afar depression (42°E). North of the main limb of the ITCZ, shallower convection occurs, restricted to between 700 and 600 hPa. Over the Nile Plains (32°E), it is associated with the low-level convergence at 17-18°N between the dry northerlies and the moist southerly monsoon flow. In the upper troposphere near 10-15°N is found a strong easterly flow, the Tropical Easterly Jet (TEJ), with speeds above 25m.s^{-1} at 150 hPa. The TEJ is a planetary scale phenomenon associated with upper tropospheric heat release over the monsoon regions of Asia and to some extent Africa. It is decelerating over north-east Africa. Slightly to the south of the TEJ core, there is clear upper tropospheric diffluence in the meridional direction, in connection with the strong ascending motion over Sudan and Ethiopia (fig.3; Hulme and Tosdevin 1989). At 42°E, over Somalia and the Indian Ocean, descending motion predominates at most levels (fig.3). The Somali jet is well shown. North of the Ahmar mountains (9.5°N), downslope winds converge with northerlies from the Red Sea along the Afar Convergence Zone, a weak lee confluence which slopes upwards to the south and is capped by weak air ascent (Tucker and Pedgley, 1977). Near 600-500 hPa, north-easterlies dominate, which result from the injection of dry warm air, mainly from the Arabian Peninsula.

In October, the Somali Jet has collapsed. Southeasterlies persist south of the equator and in northern Kenya, and the ITCZ starts to retreat to the south, towards northern Somalia where it is very diffuse, and southern Sudan. Over the Red Sea, as the southeasterlies have replaced the summer monsoon flow, the RSCZ reappears at about 17-19°N and will persist until April-May (Pedgley, 1966). Rift flows over the Red Sea are capped by a persistent inversion around 800 hPa, which inhibits vertical motion. The November wind field (fig.2) illustrates the circulation patterns at the time of peak rainfall in much of eastern equatorial Africa. The ITCZ has now shifted close to the equator, but as in April it is very diffuse. Over the Indian Ocean, converging northeasterlies and southeasterlies actually turn to westerlies along the equator. This reflects the gradient between relatively cool sea-surface temperature (SST) in the western Indian Ocean and the warmer waters around Indonesia. It decreases moisture advection towards East Africa. In addition, mid-tropospheric mean vertical motion over equatorial Eastern Africa remains weak, and convergence is found in the upper troposphere (Yang et al., 2015).

3. Local circulation features

The land surface heterogeneity arising from the contrasted topography and the presence of major waterbodies accounts for a number of local- and regional-scale winds, of importance to rainfall distribution.

In the gap between the Ethiopian and the Kenya Highlands, a strong southeasterly low-level wind was detected by Kinuthia and Asnani (1982) and termed the Turkana Jet (fig.2 and 3). This permanent jet, with mean winds around 10-12 $m.s^{-1}$ peaking at 850 hPa (Nicholson, 2015a), results from a Bernoulli effect, i.e. orographic channeling between the Ethiopian and Kenya Highlands (Sun et al., 1999; Indeje et al., 2001). It is strongest in the late night and early morning (0300 or 0900 EAT). High speeds (30 to 50 $m.s^{-1}$) were occasionally found based on pibal ascents during a field campaign in 1983-1984 (Kinuthia, 1992) but in reanalysis products wind variations are smaller. A strong divergence is found at the entrance of the jet (fig.2). Descent occurs above its core (Sun et al., 1999), especially at daytime, which is suggested to inhibit convection and contribute to the aridity of northern Kenya (Nicholson, 2015a). The jet is nevertheless important to the advection of moisture from the Indian Ocean to the Ethiopian Highlands (Viste and Sorteberg, 2013).

Another gap wind jet has recently been uncovered at the northern tip of the Ethiopian Highlands, the Tokar Gap jet (Jiang et al., 2009; Davis et al., 2015). The Tokar jet is a seasonal wind found in summer across the Sudanese coast on the Red Sea, as part of the monsoon wind flow across Sudan which feeds into the Asian monsoon flow, through a breach in the mountain ranges (fig.1 and 3b). It reaches more than 15 $m.s^{-1}$, with a distinct early morning maximum (Jiang et al., 2009). Taking the form of cross-sea southwesterly winds which last from days to weeks, it disturbs the prevailing along-sea northwesterly winds (Zhai and Bower, 2013). Pulses of the Tokar jet are related to the development of mesoscale convective systems (Davis et al. 2015).

Differential heating and cooling of the terrestrial surface at day- and night-time between elevated and low-lying areas and between land and water bodies result in widespread breeze systems across much of Eastern Africa, as exemplified in numerical experiments (Mukabana and Pielke, 1996). Sea breezes occur all along the Red Sea and Indian Ocean coasts, but have attracted few studies. Flohn (1965a) noted on both sides of the Red Sea the existence of well-defined sea breezes. In winter, in conjunction with the inversion at about 1800 m and the activity of the Red Sea Convergence Zone (Pedgley, 1966), they result into precipitating stratiform clouds on the mountain escarpments. In summer, along the Sudanese Red Sea coast a sea breeze of 3-8 $m.s^{-1}$ lasting for 2-6 hours, replaced after 2200 LST by a land breeze, often as a precursor to the Tokar jet, was found in WRF simulations (Davis et al., 2015). Further south in Kenya, Nganga and Masumba (1988) indicated that sea breezes can be detected 120 km away from the coast, and found that the breeze circulation, including the upper return flow towards the ocean, reaches a height of 2000 m. Along the flat coast of Tanzania, there is a complex interaction between the sea and land breezes and the prevailing synoptic flow. Pronounced sea breeze development occurs at Dar-es-Salaam when the synoptic flow is weak and alongshore (Sumner, 1982).

There is also evidence of major breeze systems over and around the larger lakes. Over Lake Victoria, the strong diurnal variations of surface and upper winds were recognized as early as 1908 by Arthur Berson, whose expedition incidentally discovered that the tropical tropopause was higher and colder than in the midlatitudes (Sürring, 1910). Daytime lake breezes from the cool lake surface to the heated surroundings are associated with subsidence over the lake (Flohn and Fraedrich, 1966; Anyah et al., 2006; Thiery et al 2015). East of the lake, lake breezes combine with upslope breezes on the flanks of the western Kenya Highlands to generate strong

updraughts. In conjunction with the synoptic scale easterlies, this accounts for the asymmetric pattern found between the western and the eastern part of the lake basin (Anyah et al., 2006). At night, the thermal inertia of the lake generates a low pressure anomaly, land breezes which converge towards the lake, and intense convection. Strong diurnal wind changes are also found over Lake Tanganyika, but being a Rift lake, about half of its diurnal wind variations is due to slope breezes, one quarter is strictly due to the thermal lake effect (lake breeze), while the rest of the variations result from interactions with the southeast tradewinds (Savijärvi, 1997).

Broad-scale diurnal changes in atmospheric motion across Eastern Africa are illustrated based on ERA-interim data, by plotting the afternoon minus early morning difference in zonal winds and vertical velocity (fig. 4). The cross-section along the equator for April, the wettest month at this latitude, shows enhanced rising motion in the afternoon over the highlands (eastern and western Rift areas), although over the Kenya Highlands it does not extend above 500 hPa. Afternoon rising motion is also found inland near the coastline (west of 43°E). Anomalous afternoon descending motion occurs over the Indian Ocean above 700 hPa, as well as near 39°E and over Lake Victoria (33°E). Surface lake breezes are noticeable west and east of the lake. Afternoon upslope winds occur over the eastern flank of the Kenya Highlands.

Further north along 13°N, strong diurnal changes in atmospheric motion are also found during the main Ethiopian rainy season (July, fig.4). Enhanced afternoon rising motion over the Ethiopian Highlands reflects deep convection driven by daytime heating of the elevated surface. It is fed by converging upslope low-level winds. To the west, over the Nile Plains, daytime rising motion is also found, but restricted to the low troposphere. The upper tropospheric mass excess over the Ethiopian Highlands is exported to the west via the Tropical Easterly Jet, slightly stronger in the afternoon than in the morning. Strong daytime descending motion is found in the lower troposphere over the Afar depression and Gulf of Aden.

4. Mean solar radiation and temperature patterns

Contrary to common belief, the space-time patterns of cloudiness and solar radiation in the tropics in general, and Eastern Africa in particular, do not simply reflect the ITCZ and rainbelt movements. Annual means of surface incoming shortwave radiation (fig.5), based on METEOSAT second generation (MSG) satellite data, show high values (>250 $W.m^{-2}$) over much of Eastern Africa except southern Ethiopia, the area west of Lake Victoria towards the

Congo Basin, southwestern Tanzania and isolated mountains of Kenya. The lowest solar radiation is found near Mt Ruwenzori (Uganda, 183 $W.m^{-2}$) as presumed by Griffiths (1972) although data was unavailable, and the highest solar radiation (292 $W.m^{-2}$) around Bosaso (Puntland, northern Somalia). A notable feature is the patchwork of high and low radiation values over some highland areas such as Ethiopia, reflecting convective cloud buildup over the mountain tops while valleys are often cloud free.

Seasonal regimes from MSG estimates (fig.5, top right) are compared with World Radiation Data Centre (WRDC) in situ measurements, showing a good overall agreement, although MSG data tend to overestimate actual solar radiation over parts of Kenya and Tanzania. Monthly maps (fig.5, bottom) reflect the influence of latitude, ITCZ shifts and orography, but the relationship between solar radiation and rainfall regimes is often loose. In January, maximum solar radiation is found close to the equator over the Indian Ocean, with high values (250-300 $W.m^{-2}$) in Somalia, Eastern Ethiopia, South Sudan, Northern Uganda and much of Kenya. To the east (the Democratic Republic of the Congo) and south (southern Tanzania), clouds associated with the ITCZ reduces incoming solar radiation to about 200-250 $W.m^{-2}$. Low values are also found in the north of the region, due to the shorter day length with increasing latitude. Over the central Red Sea, cloud cover associated with the RSCZ further reduces solar radiation to about 150-170 $W.m^{-2}$ (Drake and Mulugetta, 1996). In April, maximum solar radiation has shifted to the northern hemisphere, with very high values (>270 $W.m^{-2}$) everywhere north of 10°N as well as over Somalia and the equatorial Indian Ocean. The main rains over Kenya, Somalia and Eastern Ethiopia are not accompanied by a strong reduction in solar radiation (Huxley, 1965; Kuhnel, 1991), suggesting erratic, short duration convective clouds associated with the diffuse ITCZ. Low solar radiation is found on windward slopes and high elevation ranges in southern Tanzania, Rwanda, Burundi, and isolated mountains in Kenya and southern Ethiopia. In July, cloudiness associated with the ITCZ again imperfectly explains solar radiation distribution (fig.5). Very low insolation (140-200 $W.m^{-2}$) is found over much of the Ethiopian Highlands in conjunction with the main rains (only about 50 hours of sunshine per month at Addis-Ababa in summer; Fazzini et al. 2015). This partly extends to South Sudan. North of the ITCZ and in the Red Sea and Gulf of Aden trenches, dry air and a zenithal sun account for high (270-327 $W.m^{-2}$) solar radiation. Although over Tanzania, Somalia and much of Kenya the weather is dry, solar radiation is highly contrasted. Unexpectedly low values (150-220 $W.m^{-2}$) are found east of the East African highlands and in southern Somalia. They result from extensive low level stratocumulus cloud cover associated with a temperature inversion within

the southerly flow (Okoola, 1990). On windward slopes (Nairobi and Embu, fig.5, top right), the phenomenon can be exacerbated, while downwind, over the Tanzania plateau or the Turkana gap, divergence and a dried up atmosphere result in high solar radiation. In October, solar radiation maxima shift to the southern hemisphere, except west of Lake Victoria where persistent cloudiness associated with the main rains reduces solar radiation to about 180-220 $W.m^{-2}$. Further east, despite the ITCZ presence, solar radiation is quite high, as in April. A minimum persists over the Bale mountains of southern Ethiopia, in agreement with Drake and Mulugetta (1996).

Mean temperatures are evidently influenced by elevation (fig.6). Typical lapse rates in Ethiopia are 5.1°C/1000 m for maximum temperature and 6.5°C for minimum temperature (Fazzini et al 2015). As an average over Kenya, Uganda and Tanzania, they are slightly higher (5.6°C) and lower (6.3°C) for maximum and minimum temperature respectively (Griffiths, 1972). Over Mt Kilimanjaro, Appelhans et al. (2015) based on a dense station network demonstrated a clear break-point in temperature lapse rate at around 2300 m (-8.4°.km^{-1} below, -4.2°C.km^{-1} above), whatever the season. It corresponds to the average condensation level, with relative humidity decreasing both downward and upward. Lapse rates tend to slightly increase away from the equator in boreal summer and autumn (fig.6), and decrease in boreal winter. Isotherms markedly slope down towards the south in summer (July), with the 15°C isotherm found around 1500 m near 11°S while it is as high as 2800 m near 13°N. Local temperatures sometimes show significant departures from these mean patterns due to interactions between the large-scale winds and orography. East of the Kenya Highlands for instance, persistent cloudiness (81%) accounts for very low July maximum temperatures in Nairobi (21°C at 1800 m). The East African Great Lakes significantly cool air temperatures, over the lakes themselves (except Lake Kivu) and downwind of them (Thiery et al., 2015).

Eastern Africa includes the hottest known place on earth at Dallol in the Afar depression (130 m below sea level), with a 34.6°C annual mean temperature (1960-66; Pedgley 1967). The lowest mean annual temperature is -7.1°C on the Mt Kilimanjaro summit (Thompson et al., 2002). Over most of Eastern Africa, frost sporadically occurs around 2200-2400 m, although above 3500 m it becomes a recurrent, almost daily feature. In Central Kenya, maps of frost incidence based on MODIS satellite data show regular frost occurrence above 2000 m, making tea plantations at risk, with occasional occurrence along valleys at lower altitudes due to cold air drainage (Kotikot and Onywere, 2015). Over Mt Kilimanjaro, mean annual minimum

temperature reaches freezing point at 2700 m (Hemp, 2006). In austral summer, the southern Tanzania Highlands regularly record frost at much lower elevations.

As expected from an equatorial region, the mean annual temperature range is generally small (fig.7). In all of Eastern Africa except the southern highlands of Tanzania and the northern part of the region (Sudan, Red Sea, Afar depression, northern Somalia), temperatures vary by no more than 5°C. The smallest range (<2°C) is incurred along the equator in the wet and cloudy regions from the eastern DRC to western Kenya through southern Uganda, Burundi and Rwanda. In these regions, highest temperatures generally occur in February-March before the main rains (e.g., Mbarara and Embu on fig.7, right panels), while lowest temperatures are found in July-August, during the relatively dry but cloudy season. Over the Ethiopian Highlands, the annual temperature range is also small (Fazzini et al., 2015). The reason is heavy cloud cover and precipitation during summer, which depresses maximum temperature, lower in July-August than in any other season (Addis-Ababa, fig.7). The higher annual temperature range in northern Sudan and along the Red Sea and Gulf of Aden is due to the marked winter cooling and very high summer temperatures, both seasons having little cloud cover. In these regions, a simple annual cycle is found (fig.7, Dongola, Port-Sudan, Djibouti) with highest maximum temperatures (40-44°C) in June-August, and lowest minimum temperatures in January-February. The sea influence makes minimum temperatures much higher along the coast (18-22°C) than inland (Dongola 10.4°C). In central Sudan (Wad-Medani, fig.7), the temperature regime is similar except that there is a secondary minimum in summer as a result of cloudiness and rains associated with the monsoon. Highest maximum temperatures (41-42°C) occur ahead of the rainy season, around May. As in northern Sudan, Southern Tanzania temperature regimes (Songea, fig.7) show a single peak, but it is inverted due to the location in the southern hemisphere, November being the warmest month and July the coldest. On the plains facing the Indian Ocean, the annual temperature range is small; highest temperatures are generally found in March (Mandera and Dar-es-Salaam, fig.7) while lowest temperatures switch from austral winter (July) in the southern hemisphere to boreal winter (January) in the northern hemisphere. In southern and central Somalia, July is generally cooler than January due to stratiform clouds and (relatively) cool air advection by the strong cross-equatorial air flow in boreal summer. Along the eastern coast of northern Somalia, cold upwelled waters further lower air temperature: at Obbia (48.5°E, 5.3°N), maximum temperature is 28.5°C in August, the coolest month of the year (Muchiri, 2007).

The mean diurnal temperature range, between 10 and 15°C, well exceeds the annual temperature range. As expected, it is smaller during the rainy seasons (fig.7), due to the cloud cover restricting daytime warming and nighttime cooling, and at coastal stations, due to the thermal inertia of the sea. At very high elevations, diurnal cycles of solar radiation and temperature markedly differ from those of low elevations. At the Mount Kenya Global Atmospheric Watch station (3678 m amsl), morning is almost cloud-free, then convective clouds gradually build up and result into decreasing solar radiation, until clouds start to dissolve just before sunset, as upslope winds vanish (Henne et al., 2008). These diurnal cycles, very regular throughout the year, result in a temperature maximum as early as 1100 to 1300 LST, in accordance with scantier early observations made on the Lewis Glacier at 4900 m amsl (Davies et al., 1977). At a lower altitude in the Kenya Highlands, sunshine also often peaks in the morning, as convective clouds build up in the afternoon, even in the dry season. However, in areas where low level stratiform clouds occur, like in July at Nairobi, the diurnal sunshine regime is inverted, with morning clouds tending to dissipate in the afternoon (Griffiths, 1972).

5. Mean precipitation patterns

Mean annual precipitation

As much as 69% of Eastern Africa is classified as hyperarid, arid and semi-arid (UNDP/UNSO, 1997), i.e. with a mean annual precipitation (MAP) under 50% of the mean annual potential evapotranspiration (PET). Rainfall is lower than 400 mm in much of Sudan, on the Red Sea coast, in the Afar depression, and along the Gulf of Aden in northern Somalia (fig.8). Hyperarid conditions (MAP/PET ratio <0.05, i.e. annual rainfall below 100-150 mm) are even found towards the Egyptian border and near the tip of the Horn. An area receiving less than 400 mm also stretches further south from eastern Ethiopia to Lake Turkana through north-eastern Kenya. It is prolonged in the southwestern direction by a relatively dry corridor (<700 mm annually) running from eastern Kenya to central Tanzania.

On the whole, the eastern part of the region is clearly the driest, if one disregards the arid zone of northern Sudan. The predominant dryness is attached to the large seasonal amplitude of the monsoons over the Indian Ocean. It involves a quick meridional shift of the ITCZ over Eastern Africa, both in its south-north and north-south translations. Brief rainy seasons in the transition seasons leave room to quasi-meridional low level winds in both the northern winter and

northern summer, in all the regions close to the Indian Ocean. Due to the roughly north-south direction of the coastline, these winds are strongly divergent, bring low moist static energy air from the winter hemisphere, and result into seasonal dryness in the lowlands of Somalia, Eastern Ethiopia and Eastern Kenya (Flohn, 1964; Anyamba, 1988; Yang et al, 2015). The divergence is enhanced by the north-south barrier formed by the east African Highlands (Slingo et al., 2005), which additionally block the air from the Congo Basin which has a higher moist static energy. The low rainfall amount in the east, even in the rainy seasons, is also due to a year-round divergence in the mid-troposphere above 850 hPa, and mean downward motion at 500 hPa (Yang et al., 2015). In the west of the region, dry conditions are also found in northern Sudan (fig.8), but with a southward gradient of increasing rainfall which replicates the one found in Western Africa. This part of Eastern Africa is actually under the influence of the dry northerlies in winter and the southwestern African monsoon in summer, the latter being gradually shallower and bringing less rain to the north.

Only 28% of the region receives more than 1000 mm annually, in three distinct zones (fig.8): (i) the Ethiopian Highlands, (ii) the eastern Congo Basin with an extension to the Western Kenya Highlands across Uganda and Lake Victoria, and (iii) southern Tanzania, with a northern extension to the Indian Ocean coast in Kenya.

The Ethiopian Highlands stand out as a relatively wet region, but display a marked dissymmetry. Its southwestern part is the wettest, with annual rainfall around 1500 - 2000 mm, reaching 2363 mm at Masha (7.7°N, 35.5°E, a 33-yr average). Transect A (fig.9) highlights this dissymmetry. Facing the southwesterly monsoon winds, the southwestern highlands, although not the highest, are the wettest. The relatively wet Nile Plains also contrast with the (leeward) arid Afar depression and Gulf of Aden to the northeast. As a result, MAP is only weakly correlated with altitude in Ethiopia (r^2=0.42 for 58 stations; Fazzini et al. 2015). Close to the equator, transect B (fig.9), from the Congo Basin to the Indian Ocean, highlights the role played by the highlands but also shows that rainfall is very loosely related to elevation. The Congo Basin is protected by the Western Rift from the seasonal dry and stable northeasterly and southeasterly flows from the Indian Ocean, and keep wet conditions almost year round (1500-2000 mm annually). Rainfall declines eastward in the Western Rift (below 1000 mm in the Lake Albert and Lake Edward grabens). A rainfall peak is found further east over Lake Victoria (about 3000 mm at Nabuyongo Island near the center of the lake; Flohn and Burkhardt, 1985; Yin and Nicholson, 1998) and on its western shores (Bukoba, Tanzania, 2028 mm; Kalangala,

Uganda, 2174 mm). It is associated with a nocturnal convergence, over the warm water, of combined land breezes and katabatic winds, generating deep convection which subsequently drifts westward. Further east in the Kenya Highlands, rainfall maxima close to 2000 mm are attained on both the western foothills (near 35°E) and the eastern slopes. They contrast with drier conditions (about 700 mm near 36°E) in the Eastern Rift Valley rain shadow. Rainfall also decreases towards the Indian Ocean, except near the coast due to the interaction between the southeasterlies and the coastline. In Southern Tanzania (fig.8), wet conditions result from the ITCZ presence throughout the austral summer season, as well as orographic effects. The wettest area is the southern flank of Mt Rungwe, facing Lake Malawi, with MAP around 2000-3000 mm (Williamson et al., 2014). The Tanzanian coast is moderately wet, but precipitation further increases on the islands (Mafia 1879 mm, Zanzibar 1670 mm, Pemba 1610 mm) due to moisture convergence associated with sea breezes (Francis and Mahongo, 2013).

At local scales, the relief of Eastern Africa triggers very strong MAP gradients, particularly on the windward side of mountains and escarpments reached by air flows originating from nearby seas and oceans, or major lakes like Lake Malawi. As in other parts of the tropics, there is often a mid-slope precipitation maximum (Barry, 2008), and precipitation begins to decrease with elevation at quite a moderate elevation (Anders and Nesbitt, 2015). This applies to Mt Kilimanjaro in Tanzania, where MAP increases from 500 mm in the foothills to about 2000-2500 mm around 2000 m amsl on the southern slopes while the summit receives about 400 mm (Coutts, 1969; Hemp, 2001; Rohr and Killingtveit, 2003; Mölg et al., 2009; Appelhans et al., 2015). Mt Kenya, at the equator, similarly displays a clear maximum (2000-2300 mm) between 2000 and 2500 m on the eastern slopes (Thompson, 1966; Jaetzold et al., 2006). In the drier context of Eritrea (15°N), a rainfall maximum is also found along the eastern escarpment facing the Red Sea. While Massawa on the coast only receives 184 mm and Asmara, 60 km away on the plateau (2300 m), records 530 mm, an annual rainfall over 1000 mm is found on the slopes between 800 and 1500 m (for example, Fil-Fil at 850 m has a 25-yr average of 1150 mm; Fantoli, 1966). This contrasts with the overall pattern found over the Ethiopian Highlands, representative of "dry monsoon regimes" (Anders and Nesbitt, 2015), where the altitude of the precipitation maximum is as high as 2000-2500 m.

Seasonal regimes

Two main types of seasonal rainfall regimes can be identified across Eastern Africa (fig.10): single-peak regimes, represented both in the northern and southern parts of the region, and double-peak ones. In the north-west, rainfall regimes are single-peak with a boreal summer maximum (July or August; e.g., Khartoum, fig.10). The rainy season lengthens as ones moves southwards along the Nile Valley, but still with a distinct summer peak, and the dry season remains centered on boreal winter. In north-eastern Ethiopia (e.g., Kombolcha, fig.10), the summer maximum becomes sharp but it is complemented by a spring rains season (February to May) called *Belg*, or *Sugum* in the Afar depression. These spring rains result from interactions between the low-level moist easterlies from the Arabian Sea and troughs in the upper tropospheric westerlies, showing up as a bent of the subtropical jet (Habtemichael and Pedgley, 1974; Camberlin and Philippon, 2002). Southern Tanzania also exhibits single-peak regimes with a summer maximum corresponding to the ITCZ being located in the southern hemisphere (e.g., Sumbawanga, fig.10). The rainy season is quite broad, with relatively heavy rainfall amounts from November to April. On south or south-east facing slopes, like at the northern tip of Lake Malawi, the maximum is shifted towards April or May due to orographic uplift as moist southeasterlies strengthen.

The equatorial regions and most of the Indian Ocean coast plains have double-peak regimes with rains in the transition seasons (MAM and OND). The northern spring one, called the "long rains" or *Masika* in Kenya and Tanzania, or *Gu* in Somalia, is usually the main one, like at Gode, south-eastern Ethiopia (fig.10). The lower rainfall amounts found in the OND season compared to the MAM season are due to the Western Indian Ocean SST being lower in OND, which results in a slightly drier and more stable atmosphere (Yang et al., 2015) and an equatorial westerly flow from the western to the eastern Indian Ocean associated with moisture divergence near Eastern Africa. Locally, on the eastern slopes of the Kenya Highlands, and in Western Uganda, the OND "short rains" or *Vuli* rains (*Der* in Somalia) become the dominant rainy season (e.g., Kitui, fig.10). This feature is not fully explained, but may reflect the fact that the OND rains tend to be enhanced when easterlies are stronger (Camberlin and Wairoto, 1997), resulting in east-facing slopes being wetter than in MAM, where more rain is associated with westerly anomalies. Both the MAM and OND rainy seasons are short, at about 60-65 days each in Kenya (Camberlin et al. 2009) and less in much of Somalia (Liebmann et al., 2012). They are separated by two dry seasons, of which the boreal summer one (June-September) is generally the longest and driest. The boreal summer dryness is due to the dynamically stable south-easterlies (south-westerlies over Somalia) and their divergence (Flohn, 1965a; Yang et

al. 2015). However, in northern Uganda and western Kenya, a third rainfall maximum is found in boreal summer (Davies et al., 1985) as a result of mid-tropospheric moist westerlies and a low pressure anomaly (Anyamba and Kiangi, 1985) related to the secondary convergence zone shown on figure 2. The transition between the MAM rainy season and the subsequent dry season is not smooth but often consists of quite abrupt jumps, coinciding with successive stages in the development of the Somali Jet (Riddle and Cook, 2008). The cessation of the MAM rains in East Africa tends to shortly precede (10-15 days) the monsoon onset over Kerala, India, in conjunction with the Somali jet intensification (Camberlin et al., 2010).

Over the Red Sea area, rainfall is very low but regimes are complex. The most frequent pattern is a maximum in boreal winter (December-January; cf. Massawa, Eritrea, fig.10). These rains result from the Red Sea Convergence Zone (Flohn, 1965b; Pedgley, 1966). Scattered showers can also occur in spring and autumn (the main rainfall maximum along the Sudanese coast), in association with upper troughs in the westerlies, and in summer, mainly to the south along the Afar Convergence Zone (Tucker and Pedgley, 1977) like in the inland part of the Republic of Djibouti.

6. Rain-producing systems and diurnal rainfall variations

Compared to Western Africa and many other tropical areas, Eastern Africa is characterized by a low prevalence of organized disturbances (Nicholson, 1996), although there are still few comprehensive studies on the atmospheric disturbances impacting the region. Easterly waves have for long been considered as absent from Eastern Africa. Although most convective systems that trigger African Easterly Waves (AEW) originate from the region around Darfour (western Sudan), in some cases the Ethiopian Highlands play a role in initiating these systems (Mekonnen et al., 2006). Mekonnen and Rossow (2011) further found that upper-level easterly waves, propagating into East Africa from the Indian Ocean in summer, enhance convection and interact with the Ethiopian highlands to trigger organized convection affecting the initiation of low-level AEW. Some AEW giving birth to tropical cyclones in the North Atlantic can be actually traced back to periods of high lightning activity in Eastern Africa (Price et al., 2007) or mesoscale complexes from northern Ethiopia (Hill and Lin, 2003). However, long-lived precipitation episodes from the Ethiopian Highlands that survive beyond a single diurnal cycle only occur every 2-3 days (Laing et al. 2012). Mekonnen and Thorncroft (2016), considering summer convection over the region centered on Sudan, found both eastward and westward

moving disturbances, the latter with a 4-day period. A 4-5 day periodicity in central Sudan rainfall had actually been earlier detected by Hammer (1976).

Closer to the equator and for the two equatorial rainy seasons, Laing et al. (2011) noted that many mesoscale convective systems (MCS) were forming on the mountains of East Africa, as a result of thermal forcing associated with large elevated heat sources, then moving westward. MCS tend to decay during the morning, but some of them regenerate later in the afternoon. However, they are generally short-lived compared to West Africa. Convection is also modulated by eastward-moving equatorially trapped Kelvin waves. Along the Indian Ocean, Laing et al (2011) also noted a line of cold cloud parallel to the coast between 1400 and 1500 local time which moves inland in the evening, becoming more intense and broader. This pattern was attributed to the development of sea breezes.

In the southwestern Indian Ocean, easterly waves have been documented in early studies to propagate to the east African coast (Trewartha, 1961; Gichuiya, 1974), but there is a lack of recent data about them. These waves develop in the boreal summer southeasterly flow, associated with a strengthening of the Mascarene High (Okoola, 1989), although evidence was also found of westward-propagating waves in austral summer (Jury et al., 1991). Some of these waves bring heavy rains on the coasts of Kenya and Tanzania (Lumb, 1966; Fremming, 1970).

Given the equatorial location, upper tropospheric troughs do not have an influence on rainfall as conspicuous as in Southern or Northern Africa. Yet, they are a major ingredient in the spring small rains over north-eastern Ethiopia, Eritrea and the Red Sea area. Contingent upon a sustained low-level south-easterly moisture influx, they induce upper tropospheric divergence and spells of 3-5 days of heavy rains (Habtemichael and Pedgley, 1974; Kassahun, 1986). Quite similar mechanisms explain the November rainfall maximum further north around Port-Sudan (Hassan, 1986). Cases of an indirect influence of midlatitude systems on East African rainfall closer to the equator have also been reported. For instance, in austral summer, a pressure rise in the Mozambique Channel associated with a cold front results in wet conditions in central Kenya (Sissons, 1966). The occasional extension of mid-tropospheric troughs towards equatorial latitudes, leading to the replacement of subsiding easterlies by a westerly flow, is also propitious to rainfall in Kenya.

Tropical cyclones only marginally affect the extreme southeastern and northeastern parts of the region. The Tanzanian coast has occasionally been hit by westward-travelling tropical cyclones or tropical storms originating from the southwestern Indian Ocean. They mostly occur between February and May, in connection with the warmer SST and dominant southeasterly flow (Obasi, 1977). In northeastern Somalia, tropical cyclones travelling westward from the Arabian Sea very infrequently reach the coast. West of 54°E, 72% are found in October-December, and most others in May-June. They contribute to raise the average rainfall in an otherwise hyperarid zone, resulting in the rainiest month being November around cape Guardafui. Examples of tropical cyclones or tropical storms causing human and cattle losses over northern Somalia, all in November, are found in 1972, 1994, 2013 and 2015, where an unusual sequence of two cyclones (Megh and Chapala) occurred in less than 10 days.

Several of the above studies highlighted the role of terrain in the control of convection over Eastern Africa. Waterbodies also have a major effect on rainfall processes. Along the Indian Ocean coast, sea breezes play an important part in rainfall generation, shown as a band of high rainfall along the coast in Kenya (fig.8) and slightly inland in southern Somalia (Fantoli, 1965). The effect of the coast in initiating and augmenting storm rainfall is demonstrated by the fact that in Tanzania correlation fields for daily rainfall closely parallel the coast (Sumner, 1983), which reflects the interaction between sea breezes and the large-scale wind flow. Lakes also play a significant role in the rainfall regimes. Rift lakes being incised in the highlands they lie in rain shadows where rainfall is relatively low, but the major East African Great Lakes (Victoria, Tanganyika, Albert and Kivu) enhance precipitation by 732 $mm.yr^{-1}$ over their surface (Thiery et al. 2015). This is caused by the high nocturnal lakes' temperature, which generates a land breeze convergence, an unstable atmosphere, and a pronounced rainfall maximum at night, while at daytime the higher temperature over land induce lake breezes, subsidence over the lakes and no rain. However, over Lake Victoria, a northeast-southwest gradient in lake temperature is found which, in addition to asymmetries in the breeze system, contributes to higher rainfall amounts in the west than in the east (Song et al., 2004). There is little evidence of any corresponding reduction in rainfall away from the lakes, except perhaps over parts of the Lake Victoria catchment (Anyah and Semazzi 2004). Lake Tanganyika also has a noticeable effect on diurnal rainfall distribution (Nicholson and Yin, 2002). While over the lake's catchment, maximum rainfall frequency occurs between 1630 and 1930 LST, late night to early morning convection is frequent along the western lakeshore. Large swamps likewise have a noticeable impact on climate. Numerical experiments on RegCM3 regional

model show that those of South Sudan enhance (+40%) local rainfall, and to a smaller extent increase rainfall further north in central Sudan (up to +15%) through longer-lasting rain producing systems, although they have no effect on Ethiopian rainfall (Zaroug et al., 2013).

Diurnal regimes of Eastern Africa partly reflect the nature of the rain-producing systems, and the role of terrain and waterbodies (fig.11). Two main types of diurnal rainfall regimes are found in Eastern Africa: the lake and coastal regimes, with a morning peak (e.g., sites 4 and 6 on fig.11), and the land regimes, with an afternoon or evening peak (e.g., sites 1, 3, 5). Based on TRMM precipitation estimates at 3-hourly time step for 1998-2014 (Huffman et al., 2007), a broader picture of diurnal variations is shown by mapping the wettest 3-hour period (fig.11). A late afternoon maximum (1800 EAT) dominates, shortly after the maximum heating of the land surface. However, peak rainfall is earlier (1500 EAT) in the immediate hinterland along the Indian Ocean coast, in the depression from South Sudan to northern Kenya, west of Lake Victoria, around Lake Tanganyika and over the highest mountain ranges (e.g., Haile et al. 2013), suggesting early convection associated with daytime heating and the penetration of the sea breeze front (Laing et al, 2011). On the coast itself, as well as over the ocean adjacent to it, morning rains dominate in association with the land breeze front, but the peak is not as sharp as the afternoon maximum over land. Major lakes also show a distinct night to morning maximum (Nicholson and Yin, 2002; Thiery et al. 2015). A noticeable feature (fig.11 and Camberlin et al., 2017) is the evidence of a phase propagation, either from the coast towards the interior (over the lowland areas along the Indian Ocean, in eastern Kenya and Somalia, and along the Red Sea, in the Afar depression) or westwards from the highlands (from the Eritrean highlands to the Nile plains, or from central Ethiopia towards South Sudan). They account for a late evening / night maximum found over parts of northern Kenya (Tomsett, 1975) and Sudan (Pedgley, 1969, and fig.11, sites 2-3). This picture neglects some seasonal variations, especially along the coastlines where changes in the synoptic wind flow influence the timing of sea and land breezes and location of the breeze front, as around Dar-es-Salaam, Tanzania (Sumner, 1984).

The nature of rainfall processes and the influence of topography is also reflected in the distribution of daily precipitation intensities. As earlier noted for Tanzania (Jackson, 1972), it is quite different from that of mean annual rainfall. Figure 12 shows the 95th percentile (P95) of daily rainfall amounts, based on wet days only. The values computed from TRMM data (1998-2014, shadings) are compared with raingauge observations (any period, but at least 7

years of data; dots on figure 12). There is a distinct geography, with intense rainfalls in the eastern plains next to the Indian Ocean (40-60 mm in eastern Kenya, Somalia, and eastern Ethiopia) and low values over the highlands (20-30 mm in Western Kenya, the Congo-Nile watershed from Burundi to northern Uganda, the Ethiopian Highlands). The Nile Plains and the Red Sea coast have intermediate values. They also show some discrepancies between TRMM and raingauge data, with the former often underestimating actual P95. Elsewhere the the two types of data reasonably agree. Over Tanzania (not shown, Nieuwolt 1974), a similar contrast is found between the eastern part of the country, where heavy precipitation is more frequent, and the western part. The more intense rain events in the eastern plains is likely the result of higher precipitable water and, along the coast, the occurrence of organised disturbances. Exposure to the dominant winds is also an important factor. Heavy rains are common to the north of lake Malawi / Nyassa, near Mt Kilimanjaro (Nieuwolt, 1974) and on the eastern slopes of the central Kenya Highlands (fig.12), where orographic uplift combined with daytime convection cause persistent rains. The highest reported 24-hour precipitation in equatorial East Africa is actually found at coastal stations (Indian Ocean and western Lake Victoria) and on windward slopes facing southeasterly air flows, as at Tukuyu (Tanzania) on the slopes overlooking lake Malawi / Nyassa, with a record daily rainfall of 432 mm (Griffiths, 1972).

Parts of Eastern Africa singularize as having frequencies of several weather hazards close to world records. The northern and western shores of Lake Victoria record over 200 thunder days per year (Kampala, 222 days; Bukoba, 226 days). These locations do not coincide with the world's highest lightning rates, which are found in the Congo Basin, downstream of the mountain ranges of the African Rift Valley (Christian et al., 2003; Zipser et al. 2006), but they denote the recurrence of storm development associated with the diurnal cycle of convection over Lake Victoria. In Western Kenya, it is the hail frequency which is close to world records: on average there are 114 days annually where hail is reported somewhere in the region (Sansom, 1966), and point incidence of hail at Kericho Tea Research Foundation is between 18 and 30 storms annually in 6 years out of 10 (Stephens et al., 1992). Hailstorms develop from the interaction between the combined slope and lake afternoon breezes east of Lake Victoria and the synoptic-scale easterly flow, and incur major damages to tea plantations around Kericho and Nandi Hills. In Uganda, there are 5 to 10 hail occurrences a year at elevations between 1500 and 2500 m (Jameson and McCallum, 1970).

7. Rainfall variability and change

Eastern Africa undergoes large interannual rainfall variations. Given the semi-arid conditions which prevail over much of the region, the generally low incomes and the dependence to water resources which account for a high vulnerability, these variations have dramatic effects on the economy and the living of local communities. Figure 13 recalls that the tropics, except for very wet months and locations, shows much larger interannual rainfall variations than the extra-tropics (Camberlin, 2010). Equatorial East Africa (mainly Kenya and southern Somalia) adhere to this feature, and many of its wetter locations (above 150 mm/month) even exhibit larger interannual rainfall variations than in other parts of the tropics. This particularly applies to the October-December short rains, which therefore contribute disproportionately to the interannual variations of annual rainfall (Nicholson, 1996). At Wajir (Kenya) for instance, over the 89-yr period ending in 2011, 20% of the years recorded less than 50 mm of rain in OND, while on 3 occasions (1961, 1997, 2011) rainfall exceeded 500 mm, with a maximum of 891 mm in 1997.

Rainfall variations since the early 20th century are analyzed based on the CenTrends precipitation dataset (Funk et al., 2015a) and global gridded data set from the Global Precipitation Climatology Centre (GPCC, Schneider et al., 2011). Only the three main east African rainy seasons are discussed (MAM = March-May; JJAS = June-September; OND = October-December), since the January-February rains in Southern Tanzania are more related to the summer rains of Southern Africa.

March-May is the main rainy season from the Great Lakes to northern Somalia. Although the leading mode of interannual rainfall variability covers most of this region (fig.14a), it extracts a relatively small share of variance (39%) since this season shows a low spatial coherence (Ogallo, 1989; Moron et al., 2007; Camberlin et al. 2009). The temporal consistency is not very high either, with the seasonal total being mostly driven by the variability of the onset date of the rainy season (Camberlin and Okoola, 2003; Moron et al., 2013), while the month of May exhibits distinct forcings and variability (Camberlin and Philippon, 2002; Zorita and Tilya, 2002). Regionally-averaged MAM rainfall (fig.14b) is characterized by weak decadal-scale oscillations during the 20th century, although a marked decline occurred around the 1990s (Funk et al., 2008; Lyon and DeWitt, 2012; Lyon, 2014). The early part of the 21st century has been particularly dry in Somalia, eastern Ethiopia, Djibouti and Kenya, with recurrent food insecurity culminating in the humanitarian crisis of 2011. Several hypotheses have been explored to explain the recent drought trend, including increasing SSTs in the south-central Indian Ocean,

suggested to divert moisture transport into Eastern Africa (Funk et al. 2008), an increased zonal SST gradient between Indonesia and the central Pacific (Liebmann et al. 2014), enhanced upper-level easterlies (Liebmann et al., 2017) and a westward expansion of the Pacific warm pool as a result of anthropogenic climate change (Williams and Funk, 2011). Lyon (2014) found that the trend is rather a manifestation of natural multi-decadal variability of Pacific SSTs, although Rowell et al. (2015) considered that natural variability is unlikely to have been the only driver of the recent droughts. Hoell et al. (2017) support a co-action of global warming with ENSO-like decadal variability. The weakness of the overall correlations between large-scale SST patterns and MAM interannual rainfall variations in Eastern Africa (Ogallo et al., 1988; Nicholson 2015b), added to the limited spatial and temporal coherence of rainfall variability in this season, highlight the difficulty to pinpoint a single cause for the recent drought trend. While a weak ENSO signal is found in the early part of the season (Moron et al. 2013), May rainfall is highly related to the timing of the Indian monsoon onset, a late cessation of the MAM rains heralding a late monsoon onset (Camberlin et al., 2010).

June-September (JJAS), the major rainy season in the north-western part of Eastern Africa, has been characterized by a marked rainfall decrease since the 1960s (fig.15). The decrease is much more evident in the north (Sudan, Eritrea, Western Ethiopia) than in the south, and parallels the decline found in the west African Sahel at similar latitudes. There is some uncertainty as to whether the drying up has continued over the last decades. Williams et al. (2012) documented a further decline in JJAS rainfall from 1970-1989 to 1990-2009, which they attributed to the warming of the southern tropical Indian Ocean resulting in dry static energy convergence over the Greater Horn of Africa. Jury and Funk (2013) also attributed the downward rainfall trend over the period 1948-2006 to decreased ascent in the Walker circulation over the eastern Sahel. The rainfall decrease appears to be smaller or non-existent over north-eastern Ethiopia (Lanckriet et al. 2015). Rosell (2011) found an increase in the Kiremt (June-September) main rainy season over 1978-2007 over east-central Ethiopia. Viste et al. (2013) did not find any significant change in the 1970-2010 JJAS rainfall as an average over the Ethiopian summer rainfall area. In Western Ethiopia, Blue Nile river flows actually fail to show any significant decrease, in contrast to rainfall (Zaroug et al., 2014). Further south over Uganda, Diem et al. (2014) found significant precipitation decreases between 1983 and 2012, centered on boreal summer, although the strong decrease of daily rainfall intensity casts doubt on the reliability of the ARC2 satellite estimates.

Earlier work demonstrated that ENSO (El-Niño Southern Oscillation) partly controls JJAS interannual rainfall variations in Ethiopia (Beltrando and Camberlin, 1993; Seleshi and Demarée, 1995; Korecha and Barnston, 2007; Segele et al., 2009; Diro et al., 2011), Sudan (Osman and Shamseldin, 2002) and parts of Uganda and Western Kenya (Ogallo, 1988; Ogallo et al., 1988; Camberlin, 1995; Indeje et al., 2000; Philipps and McIntyre, 2000). The ENSO signal is also very clear in the Blue Nile flow (Bliss, 1925; Bhatt, 1989; Eltahir, 1996; Abtew et al., 2009; Zaroug et al., 2014). Significant correlations between the Niño 3+4 index and July-September are found over the Ethiopian Highlands (fig.16a), with many dry years coinciding with warm events in the Pacific (e.g., 1982, 1987, 1997, 2009, 2015) and wet years coinciding with cold events (e.g., 1954-55, 1964, 1973-75, 1988). The El-Niño signal over the Ethiopian Highlands is better shown at regional scale (r=-0.74 with a 1951-2015 July-September precipitation index, fig.16c) due to quite large local variations in summer rainfall anomalies. The relationship is relatively stable with time (blue squares, fig.16b). The absence of ENSO forcing in some years (e.g., 1984, 2006, 2012) is due to the influence of meridional SST gradients, mainly controlled by the South Atlantic Ocean, which explain part of the decadal-scale variations and some of the interannual excursions (Camberlin et al., 2001; Korecha and Barnston, 2007; Segele et al., 2009). For instance, the 1984 drought results from an abnormally warm South Atlantic, inducing a southward shift of the ITCZ and reduced depth of the southwesterly monsoon (Lyon, 2014). Although the contribution of the moisture flux from the Gulf of Guinea to Ethiopian rainfall is often overestimated, as most of the humidity originates from the north (Mediterranean) and the Indian Ocean (Viste and Sorteberg, 2013), the pressure gradient between the South Atlantic and the region between Egypt and India strongly controls interannual rainfall variations in Ethiopia and surrounding areas (Camberlin, 1997; Segele et al., 2009; Williams et al. 2012). A strong and significant connection between summer rainfall and both ENSO and the Indian monsoon exists further south, from South Sudan to Northern Uganda and Western Kenya (fig.16a). The difference with Ethiopia is that the decadal-scale signal in JJAS rainfall is weaker closer to the equator (for instance, the 1960s were not as wet as in Ethiopia).

The October-December rains, in contrast to the MAM rainy season, show a very strong spatial coherence, which means that an exceptionally wet (or dry) year is usually experienced simultaneously over much of Eastern Africa. This feature was noted in early work on rainfall regionalization (Ogallo, 1989; Beltrando, 1990). The leading rainfall mode (fig.17a) explains

as much as 66% of the variance, covering most of Eastern Africa. After the relatively dry conditions of the first part of the 20th century, the 1960s were very wet, followed by drier conditions in the 1970s and 1980s (fig.17b). Since then, a weak rising trend occurred (Nicholson, 2015c), contrasting with the MAM drying. The OND rains are also characterized by a skewed distribution, with many low rainfall years contrasting with outstanding wet years. The most obvious wet events are 1961 and 1997, where rainfall greater than 3 standard-deviations caused extensive floods over Eastern Africa (Flohn, 1987; Birkett et al. 1999).

A relationship between the OND rains and ENSO was demonstrated by Ogallo (1988), Farmer (1988) and Hutchinson (1992). However, it also appeared quite early that SST patterns and zonal winds over the Indian Ocean were strongly related to OND precipitation in Eastern Africa (Ogallo et al., 1988; Beltrando and Camberlin, 1993). Abnormally high rainfall was found to result from surface easterly wind anomalies along the equatorial Indian Ocean, low-level moisture convergence and ascent over East Africa (with opposite anomalies in the upper troposphere and Indonesia, respectively), as part of the closed Walker cell circulation occurring over the Indian Ocean at this time of the year (Hastenrath et al. 1993; Hastenrath 2000). With the identification of a distinct mode of variability in the east-west SST gradients across the Indian Ocean (Saji et al., 1999), termed the Indian Ocean Dipole or the Indian Ocean Zonal Mode (IOZM), the key role of Indian Ocean SSTs was recognized (Behera et al., 2005). Ummenhofer et al. (2009) demonstrated that enhanced East African "short rains" were mainly driven by the warm SST anomalies in the western Indian Ocean (warm pole of the IOZM). Liebmann et al. (2014) actually found that the October-December precipitation increase during the period 1979-2012 was a result of the Indian Ocean warming being stronger in the west than in the east. The strength of the southern Indian Ocean south-easterly tradewinds (Mutai et al., 2012) and the location of the Mascarene High (Manatsa et al., 2013) also separately affect the interannual variations of OND rainfall. The IOZM signal in East African precipitation is quite uniform (fig.18a). However, it is uneasy to disentangle the separate contribution of IOZM and ENSO given that these two modes of variability are strongly related. Most east African wet years coincide with warm anomalies in both the IOZM and Niño 3+4 times-series (fig.18c; Black et al., 2003). It is only in some years like 1961 and 1967 that a Walker-type circulation anomaly disconnected from that of the Pacific Ocean is found in the Indian Ocean, resulting in a wet East Africa despite the absence of an El-Niño event. Some years (e.g., 1987) also do not fit the relationship with neither the IOZM nor ENSO. Clark et al (2003) actually noted that the SST–rainfall correlation broke down between 1983 and 1993. Nicholson (2015c) also found

major regime shifts in the coupled IOZM/ENSO/East African rainfall association, in accordance with Manatsa and Behera (2013), and demonstrated that the relationship between the interannual variability of the OND rains is more closely related to the zonal winds over the equatorial Indian Ocean than to either ENSO or the IOZM.

East African rainfall is also affected by intraseasonal (20-60 days) variations. The influence of the Madden-Julian Oscillation (MJO) over Kenya was first suggested by Mutai and Ward (2000), based on the west-east propagation of 850- and 200-hPa wind anomalies associated with 5-day rainfall composites. An objective signature of the MJO, based on the multivariate index defined by Wheeler and Hendon (2004), was later found in Eastern Equatorial Africa rainfall in both the March-May and October-December rainy seasons (Pohl and Camberlin, 2006a & b; Omeny et al., 2008; Berhane and Zaitchik, 2014; Hogan et al., 2015). Phases 2 to 4 of the oscillation, with reduced convection in the Western Pacific, exhibit enhanced rainfall in the Kenya Highlands and lake Victoria region, while phases 6 to 8, with stronger convection in the Western Pacific, show suppressed rainfall. This applies to heavy rainfall events in Western Kenya (fig.19), 78% of which occur during phases 1 to 4 (excluding events coinciding with an inactive MJO) and 22% only during phases 5 to 8. The rainfall enhancement in phases 3-4, while the main convective center is already over the Indian Ocean, is a result of the location of a 200-hPa trough associated with the MJO wave-like structure over the Kenya Highlands, which destabilizes the atmosphere (Hogan et al., 2015). In the lower troposphere, the low pressure anomaly over the Indian Ocean produces a pressure gradient that weakens the easterlies over East Africa, possibly replacing them by westerlies (Pohl and Camberlin, 2006a; Berhane and Zaitchik, 2014). Westerly anomalies are known to be related to wet spells over Equatorial East Africa, in March-May especially (fig.19 and Johnson and Mörth, 1960; Nakamura, 1968; Okoola, 1999; Chan et al., 2008). Although it may seem counterintuitive that a reduced moisture flux from the Indian Ocean would result into wet anomalies, the westerlies actually break the mid-tropospheric inversion (near 700-600 hPa) commonly found in the easterlies, and associated stability. Unexpectedly, a more or less opposite pattern is found along the coastline, with wet conditions in MJO phases 6-8 (Pohl and Camberlin, 2006a; Hogan et al. 2015). This pattern is suggested to result from enhanced moisture advection from the Indian Ocean, generating shallow convection and stratiform rainfall. There is no clear MJO signal in boreal summer rainfall in Eastern Africa, except over Lake Victoria where precipitation is enhanced in phase 3 and suppressed in phase 7, similar to the other seasons (Hogan et al., 2015).

8. Temperature change

Temperature changes across Eastern Africa are still poorly documented, with global temperature data sets showing gaps in the region or lacking reliability due to interpolation from few stations (Collins, 2011). King'uyu et al. (2000), based on data at 71 stations in eastern and southern Africa, found large geographical variations in observed temperature trends between 1939 and 1992, although a nighttime temperature increase dominated. Trends of temperature extremes over the greater Horn of Africa in general (Omondi et al. 2014) and Ethiopia in particular (Mekasha et al. 2014) show large spatial variations among stations, even within a given eco-environment. At national level however, all studies show a marked increase of minimal temperatures in the last 30 to 60 years, and sometimes also an increase of maximum temperatures. Ozer and Mahamoud (2013) reported a +1.24°C mean temperature increase at Djibouti between 1966 and 2011. For Sudan, Elagib and Mansel (2000) found a significant warming between 1941 and 1996 in the central and southern parts of the country. As an average over Ethiopia, Fazzini et al. (2015) found a +1.1°C increase from 1980 to 2010, for both maximum and minimum temperatures, although over a longer period (1953-2010) and based on 8 main meteorological stations with long series, the rate of minimum temperature increase is twice that of maximum temperature. Over the period 1951-2006, a separate assessment by the Ethiopian National Meteorological Agency quote a rise of +2°C, based on 40 stations (NMA, 2007). Christy et al. (2009), based on a thorough analysis of 100-yr of station data across Kenya and Tanzania, including an adjustment for inhomogeneities in the time-series, noted strong increases for minimum temperature (Tn) but much smaller for maximum temperature (Tx) whose rising became substantial only in the last (1979-2004) sub-period. Differences between Tx and Tn trends were interpreted as a response to complex changes in the boundary layer dynamics, with Tx being influenced by the daytime vertical connection to the deep atmosphere whereas Tn represents only a shallow layer. Similar results were obtained for Uganda (Christy 2013) across the twentieth century. Collins (2011) analysed African temperature changes between the 1979-1994 and 1995-2010 sub-periods, based on Microwave Sounding Unit (MSU) lower-tropospheric data, and found a significant warming along the coasts of Eastern Africa in March-May (+0.3 to 0.6°C) and September-November (+0.2 to 0.3°C).

Using available daily station rainfall data and two global gridded products (CRU [Harris et al. 2014] and Berkeley Earth [Rohde et al. 2013]), there is a fair agreement on the spatially

averaged temperature trend across Eastern Africa (table 1). Between 1953 and 2013, annual mean Tn increased markedly (+1.4 to 1.45°C, slightly less in the CRU data set). However, the Tx increase was almost as strong (+1.1 to 1.2°C, and +1.28°C in the CRU data set). By seasons (figure 20), as an average over Eastern Africa, June-September shows the largest increases (for both Tx and Tn), but the trends do not strongly differ in the other seasons. Increases in minimum temperatures are generally stronger (Camberlin, 2017). The trends are fairly linear, although there is also a marked interannual variability, with warmest years often coinciding with drought years, at least for maximum temperatures.

The glacier recession observed on Mt Kilimanjaro (Thompson et al., 2009) cannot be directly attributed to rising air temperatures, since temperature at glacier level remains well below freezing and 500 hPa temperature does not show any warming trend (Cullen et al., 2006). Other explanations concentrate on decreasing precipitation and cloud cover, inducing higher shortwave solar radiation (Mölg et al., 2008; Pepin et al., 2014) but the recession may also be due to pre-20th century climate shifts (Cullen et al. 2006). Over the Rwenzori Mountains (Uganda), glacier recession has been attributed to rising air temperatures (Taylor et al., 2006). However Mölg et al. (2006) challenged this assumption, since 600 hPa air temperatures do not show any significant trend in NCEP/NCAR reanalyses over 1948–2005, while specific humidity does show a significant decrease, suggesting that drier conditions rather than warmer conditions may have been the trigger.

The recent trends of Eastern Africa climate must be considered bearing in mind longer-term trends, including those found since the 19th century and those projected for the coming decades as a result of anthropogenic climate change. However, high uncertainty remains for future precipitation trends in the region (e.g., Rowell et al., 2015).

References

Abtew, W., Melesse, A. M., & Dessalegne, T. (2009). El Niño southern oscillation link to the Blue Nile River Basin hydrology. *Hydrological Processes*, 23(26), 3653-3660.

Alter, R. E., Im, E. S., & Eltahir, E. A. (2015). Rainfall consistently enhanced around the Gezira Scheme in East Africa due to irrigation. *Nature Geoscience*. 8, 763–767, doi:10.1038/ngeo2514

Anders, A. M., & Nesbitt, S. W. (2015). Altitudinal Precipitation Gradients in the Tropics from Tropical Rainfall Measuring Mission (TRMM) Precipitation Radar. *Journal of Hydrometeorology*, *16*(1), 441-448.

Anderson, D. L. (1976). The low-level jet as a western boundary current. *Monthly Weather Review*, *104*(7), 907-921.

Anyah, R. O., & Semazzi, F. H. M. (2004). Simulation of the sensitivity of Lake Victoria basin climate to lake surface temperatures. *Theoretical and Applied Climatology*, *79*(1-2), 55-69.

Anyah, R. O., Semazzi, F. H., & Xie, L. (2006). Simulated physical mechanisms associated with climate variability over Lake Victoria Basin in East Africa. *Monthly Weather Review*, *134*(12), 3588-3609.

Anyamba, E.K. (1988). Some aspects of the origin of rainfall deficiency in East Africa. WMO, Tropical Met. Res. Program, Report series n° 28, 196-198.

Anyamba, E. K., & Kiangi, P. M. R. (1985). Mean motion field in East Africa at the level of the East African low level jet core. *Archives for meteorology, geophysics, and bioclimatology, Series B*, *36*(1), 29-41.

Appelhans, T., Mwangomo, E., Otte, I., Detsch, F., Nauss, T., & Hemp, A. (2015). Eco-meteorological characteristics of the southern slopes of Kilimanjaro, Tanzania. *International Journal of Climatology*. DOI: 10.1002/joc.4552

Asnani, G.C. (1993). *Tropical Meteorology*. Indian Institute of Tropical Meteorology, Poona, 1202 p.

Barry, R. G. (2008). *Mountain weather and climate*. Cambridge University Press, Cambridge, UK. 506 p.

Behera, S.K., Luo, J.J., Masson, S., Delécluse, P., Gualdi, S., Navarra, A., & Yamagata, T. (2005). Paramount impact of the Indian Ocean Dipole on the East African short rains: a CGCM study. *J.Climate*, 18,21 4514-4530.

Beltrando, G. (1990) Space-time variability of rainfall in April and October-November over East Africa during the period 1932-83. *J. Climatology*, 10, 691-702.

Beltrando, G., & Camberlin, P. (1993). Interannual variability of rainfall in the Eastern Horn of Africa and indicators of atmospheric circulation. *Int. J. Climatology*, 13, 533-546.

Berhane, F., & Zaitchik, B. (2014). Modulation of Daily Precipitation over East Africa by the Madden–Julian Oscillation. *Journal of Climate*, 27(15), 6016-6034. http://doi.org/10.1175/JCLI-D-13-00693.1

Bhatt, U. S. (1989). Circulation regimes of rainfall anomalies in the African-South Asian monsoon belt. *Journal of Climate*, *2*(10), 1133-1144.

Birkett, C., Murtugudde, R., & Allan, T. (1999). Indian Ocean climate event brings floods to East Africa's lakes and the Sudd Marsh. *Geophysical Research Letters*, *26*(8), 1031-1034

Black, E., Slingo, J., Sperber, K.R. (2003). An observational study of the relationship between excessively strong short rains in Coastal East Africa and Indian Ocean SST. *Mon Wea Rev* 131: 74-94.

Bliss, E. W. (1925). The Nile flood and world weather. *Memoirs of the Royal Meteorological Society* 4: 53-84.

Brink, A. B., Bodart, C., Brodsky, L., Defourney, P., Ernst, C., Donney, F., ... & Tuckova, K. (2014). Anthropogenic pressure in East Africa—monitoring 20 years of land cover changes by means of medium resolution satellite data. *International Journal of Applied Earth Observation and Geoinformation*, *28*, 60-69.

Camberlin, P. (1995). June-september rainfall in north-eastern Africa and atmospheric signals over the tropics: A zonal perspective. *International Journal of Climatology*, 15(7), 773-783.

Camberlin, P. (1997). Rainfall anomalies in the source region of the Nile and their connection with the Indian summer monsoon. *Journal of Climate* 10: 1380-1392.

Camberlin, P. (2010). More variable tropical climates have a slower demographic growth. *Climate Research*, *41*, 157-167.

:

Camberlin, P. (2017). Temperature trends and variability in the Greater Horn of Africa: interactions with precipitation. *Climate Dynamics*, 48(1), 477‑498. https://doi.org/10.1007/s00382-016-3088-5

Camberlin, P., Gitau, W., Planchon, O., Dubreuil, V., Funatsu, B. M. & Philippon, N. (2017). Major role of water bodies on diurnal precipitation regimes in Eastern Africa. *International Journal of Climatology*, in press, doi:10.1002/joc.5197

Camberlin, P., Janicot, S., & Poccard, I. (2001). Seasonality and atmospheric dynamics of the teleconnection between African rainfall and tropical sea-surface temperature: Atlantic vs. ENSO. *International Journal of Climatology*, *21*(8), 973-1005.

Camberlin, P., & Okoola, R.E. (2003). The onset and cessation of the 'long rains' in eastern Africa and their interannual variability. *Theor Appl Climatol* 75: 43-54

Camberlin, P., & Philippon, N. (2002). The east African March-May rainy season: associated atmospheric dynamics and predictability over the 1968-97 period. *J Climate*, 15: 1002-1019.

Camberlin, P., & Wairoto, J. G. (1997). Intraseasonal wind anomalies related to wet and dry spells during the "long" and "short" rainy seasons in Kenya. *Theoretical and applied climatology*, *58*(1-2), 57-69.

Camberlin, P., Moron, V., Okoola, R., Philippon, N., & Gitau, W. (2009). Components of rainy seasons' variability in Equatorial East Africa: onset, cessation, rainfall frequency and intensity. *Theoretical and Applied Climatology*, 98(3-4), 237‑249. http://doi.org/10.1007/s00704-009-0113-1

Camberlin, P., Fontaine, B., Louvet, S., Oettli, P., & Valimba, P. (2010). Climate Adjustments over Africa Accompanying the Indian Monsoon Onset. *Journal of Climate*, 23(8), 2047‑2064. http://doi.org/10.1175/2009JCLI3302.1

Chakraborty, A., Nanjundiah, R. S., & Srinivasan, J. (2009). Impact of African orography and the Indian summer monsoon on the low-level Somali jet. *International Journal of Climatology*, *29*(7), 983-992.

Chan, R. Y., Vuille, M., Hardy, D. R., & Bradley, R. S. (2008). Intraseasonal precipitation variability on Kilimanjaro and the East African region and its relationship to the large-scale circulation. Theoretical and Applied Climatology, 93(3-4), 149‑165. http://doi.org/10.1007/s00704-007-0338-9

Christian, H. J., Blakeslee, R. J., Boccippio, D. J., Boeck, W. L., Buechler, D. E., Driscoll, K. T., ... & Stewart, M. F. (2003). Global frequency and distribution of lightning as observed from space by the Optical Transient Detector. *Journal of Geophysical Research: Atmospheres*, *108*(D1).

Christy, J.R. (2013). Monthly Temperature Observations for Uganda. J Appl Meteor Climatol 52, 2363–2372. doi:10.1175/JAMC-D-13-012.1

Christy, J.R., Norris, W.B., & McNider, R.T. (2009). Surface Temperature Variations in East Africa and Possible Causes. J Climate 22, 3342–3356. doi:10.1175/2008JCLI2726.1

Clark, C. O., Webster, P. J., & Cole, J. E. (2003). Interdecadal variability of the relationship between the Indian Ocean zonal mode and East African coastal rainfall anomalies. *Journal of Climate*, *16*(3), 548-554.

Collins, J.M. (2011). Temperature variability over Africa. *J Climate* 24(14), 3649-3666.

Coutts, H. H. (1969). Rainfall of the Kilimanjaro area. *Weather*, *24*(2), 66-69.

Cullen, N. J., Mölg, T., Kaser, G., Hussein, K., Steffen, K., & Hardy, D. R. (2006). Kilimanjaro Glaciers: Recent areal extent from satellite data and new interpretation of observed 20th century retreat rates. *Geophysical Research Letters*, *33*(16).

Davenport, D. C., & Hudson, J. P. (1967). Meteorological observations and Penman estimates along a 17-km transect in the Sudan Gezira. *Agricultural Meteorology*, 4(6), 405-414.

Davies, T. D., Vincent, C. E., & Beresford, A. K. C. (1985). July-August rainfall in West-Central Kenya. *Journal of climatology*, *5*(1), 17-33.

Davies, T. D., Brimblecombe, P., & Vincent, C. E. (1977). The daily cycle of weather on Mount Kenya. *Weather*, 32: 406–417.

Davis, S. R., Pratt, L. J., & Jiang, H. (2015). The Tokar Gap Jet: Regional Circulation, Diurnal Variability and Moisture Transport based on Numerical Simulations. *Journal of Climate*, (2015).

Diem, J. E., Hartter, J., Ryan, S. J., & Palace, M. W. (2014). Validation of satellite rainfall products for western Uganda. *Journal of Hydrometeorology*, *15*(5), 2030-2038.

Diro, G. T., Grimes, D. I. F., & Black, E. (2011). Teleconnections between Ethiopian summer rainfall and sea surface temperature: part I—observation and modelling. *Climate dynamics*, *37*(1-2), 103-119.

Drake, F., & Mulugetta, Y. (1996). Assessment of solar and wind energy resources in Ethiopia. I. Solar energy. *Solar energy*, 57(3), 205-217.

Elagib, N.A., &Mansell, M.G. (2000). Recent trends and anomalies in mean seasonal and annual temperatures over Sudan. *J Arid Environments* 45, 263–288. doi:10.1006/jare.2000.0639

Elagib, N. A. (2011). Evolution of urban heat island in Khartoum. *Int. J. Climatol*., 31: 1377–1388. doi:10.1002/joc.2159

Eltahir, E. A. (1996). El Niño and the natural variability in the flow of the Nile River. *Water Resources Research*, *32*(1), 131-137.

Fantoli, A. (1965). *Contributo alla climatologia della Somalia*. Ministeri degli Affari Esteri, Rome, 478 p.

Fantoli, A. (1966). *Contributo alla climatologia dell'Eritrea*. Ministeri degli Affari Esteri, Rome, 230 p.

Farmer, G. (1988). Seasonal forecasting of the Kenya Coast short rains 1901-84. *Journal of climatology*, 8, 489-497.

Fazzini, M., Bisci, C., & Billi, P. (2015). The Climate of Ethiopia. In *Landscapes and Landforms of Ethiopia* (pp. 65-87). Springer Netherlands.

Findlater, J. (1969). A major low-level air current near the Indian Ocean during the northern summer. *Quarterly Journal of the Royal Meteorological Society*, *95*(404), 362-380.

Flohn, H. (1964). Über die Ursachen der Aridität Nordost-Afrikas. *Würzburger Geographische Arbeiten*, 12, 25-44.

Flohn, H. (1965a). Contributions to the synoptic climatology of North-East Africa. *WMO Technical notes*, 69, 236-244.

Flohn, H. (1965b). Klimaprobleme am Roten Meer. *Erdkunde*, *19*(3), 179-191.

Flohn, H. (1987). East African rains of 1961/62 and the abrupt change of the White Nile discharge. *Palaeoecology of Africa* 18: 3-18.

Flohn, H. & Burkhardt, Th. (1985). Nile runoff at Aswan and Lake Victoria: a case of discontinuous climate time series. *Z. Gletscherkunde Glazialgeol*., 21, 125-130.

Flohn, H., & Fraedrich, K. (1966). Tagesperiodische zirkulation und niederschlagsverteilung am Victoria-See (Ostafrika). *Meteorologische Rundschau*, *19*(6), 157-165.

Francis, J., & Mahongo, S. B. (2013). Analysis of rainfall variations and trends in coastal Tanzania. *Western Indian Ocean Journal of Marine Science*, *11*(2), 121-133.

Fremming, D. (1970). *Notes on an easterly disturbance affecting East Africa, 5-7 September 1967*. East African Meteorological Department Techn. Memo., 13, 13p.

Funk, C., Nicholson, S. E., Landsfeld, M., Klotter, D., Peterson, P., & Harrison, L. (2015a). The Centennial Trends Greater Horn of Africa precipitation dataset. Scientific Data, 2, 150050. http://doi.org/10.1038/sdata.2015.50.

Funk, C., Peterson, P., Landsfeld, M., Pedreros, D., Verdin, J., Shukla, S., ... & Michaelsen, J. (2015b). The climate hazards infrared precipitation with stations—a new environmental record for monitoring extremes. *Scientific data*, *2*, 150066. doi:10.1038/sdata.2015.66

Gichuiya, S.N. (1974). Easterly disturbances in the South-East monsoon. East Afr. Met. Dep. Technical Memorandum n°21, 7 p.

Griffiths, J.F. (1972). Eastern Africa. In *World Survey of Climatology*, vol.10, Griffiths J.F. (Ed.), Elsevier, 313-332.

Habtemichael, A., & Pedgley, D.E. (1974). Synoptic case-study of spring rains in Eritrea. *Arch Met Geophys Biokl*, Ser. A, 3-4, 285-296

Haile, A. T., Habib, E., Elsaadani, M., & Rientjes, T. (2013). Inter-comparison of satellite rainfall products for representing rainfall diurnal cycle over the Nile basin. *International journal of applied earth observation and geoinformation*, *21*, 230-240.

Hammer, R.M. (1970). Cloud development and distribution around Khartoum. *Weather*, 9, 411-414.

Hammer, R.M. (1976). Rainfall characteristics in Eastern Sahel. *Nature*, 263, 48-50.

Harris, I., Jones, P.D., Osborn, T.J., & Lister, D.H. (2014). Updated high-resolution grids of monthly climatic observations – the CRU TS3.10 Dataset. *Int. J. Climatol.*, 34: 623–642. doi:10.1002/joc.3711

Hassan, H.M. (1986). Favourite synoptic conditions leading to precipitation at the Red Sea coastal area of the Sudan. In *Local weather systems prediction for the Red Sea countries*, WMO, TMRP Report Series n°29.

Hastenrath, S. (2000). Zonal circulations over the equatorial Indian Ocean. *Journal of Climate*, *13*(15), 2746-2756.

Hastenrath, S, Nicklis, A., & Greischar, L. (1993). Atmospheric-hydrospheric mechanisms of climate anomalies in the western equatorial Indian Ocean. *J Geophys Res*, 98: 20 219-20 235.

Hemp, A. (2001). Ecology of the pteridophytes on the southern slopes of Mt. Kilimanjaro. Part II: Habitat selection. *Plant biology*, *3*(5), 493-523.

Hemp, A. (2006). Continuum or zonation? Altitudinal gradients in the forest vegetation of Mt. Kilimanjaro. *Plant Ecology*, *184*(1), 27-42.

Henne, S., Junkermann, W., Kariuki, J. M., Aseyo, J., & Klausen, J. (2008). Mount Kenya Global Atmosphere Watch Station (MKN): Installation and Meteorological Characterization. *Journal of Applied Meteorology and Climatology*, *47*(11), 2946-2962.

Hijmans, R. J., Cameron, S. E., Parra, J. L., Jones, P. G., & Jarvis, A. (2005). Very high resolution interpolated climate surfaces for global land areas. *International journal of climatology*, 25(15), 1965-1978.

Hill, C. M., & Lin, Y.L. *(*2003*).* Initiation of a mesoscale convective complex over the Ethiopian Highlands preceding the genesis of Hurricane Alberto (2000). *Geophys. Res. Lett.*, 30, *1232*, *doi:*10.1029/2002GL016655, 5.

Hills, R. C. (1979). The structure of the inter-tropical convergence zone in equatorial Africa and its relationship to East African rainfall. *Transactions of the Institute of British Geographers*, 329-352.

Hoell, A., Hoerling, M., Eischeid, J., Quan, X.-W., & Liebmann, B. (2016). Reconciling Theories for Human and Natural Attribution of Recent East Africa Drying. *Journal of Climate* 30(6), 1939‑1957. https://doi.org/10.1175/JCLI-D-16-0558.1

Hogan, E., Shelly, A. & Xavier, P. (2015). The observed and modelled influence of the Madden–Julian Oscillation on East African rainfall. *Met. Apps*, 22: 459–469. doi: 10.1002/met.1475

Huffman, G. J., Bolvin, D. T., Nelkin, E. J., Wolff, D. B., Adler, R. F., Gu, G., ... & Stocker, E. F. (2007). The TRMM multisatellite precipitation analysis (TMPA): Quasi-global, multiyear, combined-sensor precipitation estimates at fine scales. *Journal of Hydrometeorology*, *8*(1), 38-55.

Hulme, M., & Tosdevin, N. (1989). The tropical easterly jet and Sudan rainfall: a review. *Theoretical and applied climatology*, *39*(4), 179-187.

Huxley, P. A. (1965). A simple method for displaying diurnal patterns of cloudiness with some examples from East Africa. *Agricultural Meteorology*, *2*(1), 17-25.

Indeje M., F. H. M. Semazzi & L. J. Ogallo, 2000. ENSO signals in East African rainfall seasons. *International Journal of Climatology* 20: 19-46.

Indeje, M., Semazzi, F. H., Xie, L., & Ogallo, L. J. (2001). Mechanistic model simulations of the East African climate using NCAR regional climate model: influence of large-scale orography on the Turkana low-level jet. *Journal of Climate*, *14*(12), 2710-2724.

Jackson, I.J. (1972). Mean daily rainfall intensity and number of rain days over Tanzania. *Geografiska Annaler*, 54A, 3-4, 36-375.

Jaetzold, R., Schmidt, H., Hrnetz, B., & Shisanya, C. (2006). Farm management handbook Vol II, Part C, East Kenya. *Subpart C1, Eastern Province. Ministry of Agriculture, Nairobi Kenya*.

Jameson, J.D. & McCallum, D. *(*1970*).* *'*Climate*', in* Jameson, J.D. *(ed.), Agriculture in Uganda*, 2nd edn, Oxford University Press, Oxford, 12–23.

Jiang, H., J. T. Farrar, R. C. Beardsley, R. Chen, and C. Chen (2009). Zonal surface wind jets across the Red Sea due to mountain gap forcing along both sides of the Red Sea, *Geophys. Res. Lett*., 36, L19605, doi:10.1029/2009GL040008.

Johnson, D.H., Mörth, H.T. (1960). Forecasting research in East Africa. In *Tropical Meteorology in Africa*. Bargman D.J., Editor. WMO/Munitalp Foundation, Nairobi. 56-132.

Jury, M. R., Pathack, B., Campbell, G., Wang, B., & Landman, W. (1991). Transient convective waves in the tropical SW Indian Ocean. *Meteorology and Atmospheric Physics*, *47*(1), 27-36.

Jury, M. R., & Funk, C. (2013). Climatic trends over Ethiopia: regional signals and drivers. *International Journal of Climatology*, *33*(8), 1924-1935.

Kassahun, B. (1986). Local weather systems over the Red Sea area. In *Local weather systems prediction for the Red Sea countries*, WMO, TMRP Report Series n°29, 1-18.

King'uyu, S. M., Ogallo, L. J. , Anyamba, E.K. (2000). Recent trends of minimum and maximum surface temperatures over Eastern Africa. *Journal of Climate* 13 (16): 2876-2886.

Kinuthia, J. H. (1992). Horizontal and vertical structure of the Lake Turkana jet. *Journal of applied meteorology*, *31*(11), 1248-1274.

Kinuthia, J. H., & Asnani, G.C. (1982). A newly found jet in North Kenya (Turkana Channel). *Monthly Weather Review* 110: 1722-1727.

Korecha, D., & Barnston, A.G. (2007). Predictability of June–September Rainfall in Ethiopia. *Mon. Wea. Rev.*, **135**, 628–650.

Kotikot, S. M., & Onywere, S. M. (2015). Application of GIS and remote sensing techniques in frost risk mapping for mitigating agricultural losses in the Aberdare ecosystem, Kenya. *Geocarto International*, *30*(1), 104-121.

Krishnamurti, T. N., & Bhalme, H. N. (1976). Oscillations of a monsoon system. Part I. Observational aspects. *Journal of the Atmospheric Sciences*, *33*(10), 1937-1954.

Kuhnel, I. (1991). Cloudiness fluctuations over eastern Africa. *Meteorology and Atmospheric Physics*, *46*(3-4), 185-195.

Laing, A. G., Carbone, R. E., & Levizzani, V. (2011). Cycles and propagation of deep convection over equatorial Africa. *Monthly Weather Review*, *139*(9), 2832-2853.

Laing, A.G, Trier, S.B., & Davis, C.A., (2012). Numerical Simulation of Episodes of Organized Convection in Tropical Northern Africa. *Mon. Wea. Rev.*, **140**, 2874–2886.

Lanckriet, S., Frankl, A., Adgo, E., Termonia, P., & Nyssen, J. (2015). Droughts related to quasi-global oscillations: a diagnostic teleconnection analysis in North Ethiopia. *International Journal of Climatology*, *35*(7), 1534-1542.

Lawrimore, J. H., Menne, M. J., Gleason, B. E. , Williams, C. N. , Wuertz, D. B. , Vose, R. S. & Rennie, J. (2011). An overview of the Global Historical Climatology Network monthly mean temperature data set, version 3, *J. Geophys. Res.*, 116, D19121, doi:10.1029/2011JD016187.

Liebmann, B., Bladé, I., Kiladis, G. N., Carvalho, L. M., B. Senay, G., Allured, D., ... & Funk, C. (2012). Seasonality of African precipitation from 1996 to 2009. *Journal of Climate*, *25*(12), 4304-4322.

Liebmann, B., Hoerling, M.P., Funk, C., Bladé, I., Dole, R.M., Allured, D., Quan, X., Pegion, P., & Eischeid, J.K. (2014) Understanding Recent Eastern Horn of Africa Rainfall Variability and Change. *J Climate* 27, 8630–8645.

Liebmann, B., Bladé, I., Funk, C., Allured, D., Quan, X.-W., Hoerling, M., Thiaw, W. M. (2017). Climatology and Interannual Variability of Boreal Spring Wet Season Precipitation in the Eastern Horn of Africa and Implications for Its Recent Decline. *J Climate* 30(10), 3867‑3886.

Lumb, F. E. (1966). Synoptic disturbances causing rainy periods along East African coast. *Meteorological Magazine*, *95*(1126), 150.

Lyon, B. (2014). Seasonal drought in the Greater Horn of Africa and its recent increase during the March–May long rains. *Journal of Climate*, *27*(21), 7953-7975.

Lyon, B., & DeWitt, D.G. (2012). A recent and abrupt decline in the East African long rains. *Geophys Res Lett* 39, doi:10.1029/2011GL050337

Makokha, G.L. & Shisanya, C.A. (2010). Trends in Mean Annual Minimum and Maximum Near Surface Temperature in Nairobi City, Kenya. *Advances in Meteorology*, doi:10.1155/2010/676041.

Manatsa, D., & Behera, S.K. (2013). On the epochal strengthening in the relationship between rainfall of East Africa and IOD. *J. Clim.* **26**:5655–5673.

Mayaux, P., Bartholomé, E., Fritz, S., & Belward, A. (2004). A new land-cover map of Africa for the year 2000. *Journal of Biogeography*, *31*(6), 861-877.

McCann, J.C. (1995). *People of the Plow: An Agricultural History of Ethiopia*, 1800–1990. The University of Wisconsin Press: Wisconsin.

McHugh, M. J., & Rogers, J. C. (2001). North Atlantic Oscillation influence on precipitation variability around the Southeast African Convergence Zone. *Journal of Climate* 14: 3631-3642.

Mekasha, A., Tesfaye, K., & Duncan, A. J. (2014). Trends in daily observed temperature and precipitation extremes over three Ethiopian eco-environments. *International Journal of Climatology*, *34*(6), 1990-1999.

Mekonnen, A., Thorncroft, C. D., & Aiyyer, A.R. (2006). Analysis of Convection and Its Association with African Easterly Waves. *Journal of Climate* 19: 5405-5421

Mekonnen, A., & Rossow, W.B. (2011). The interaction between dep convection and easterly waves over Tropical North Africa: A Weather State perspective, *J. Climate*, 24, 4276-4294.

Mekonnen, A., & Thorncroft, C. D. (2016). On mechanisms that determine synoptic time scale convection over East Africa. *International Journal of Climatology*. DOI: 10.1002/joc.4614

Menne, M.J., Durre, I., Vose, R.S., Gleason, B.E., & Houston, T.G. (2012). An overview of the Global Historical Climatology Network-Daily Database. *Journal of Atmospheric and Oceanic Technology* 29, 897-910.

Mölg, T., Cullen, N. J., Hardy, D. R., Kaser, G., & Klok, L. (2008). Mass balance of a slope glacier on Kilimanjaro and its sensitivity to climate. *International Journal of Climatology*, *28*(7), 881-892.

Mölg, T., Cullen, N. J., Hardy, D. R., Winkler, M., & Kaser, G. (2009). Quantifying climate change in the tropical midtroposphere over East Africa from glacier shrinkage on Kilimanjaro. *Journal of Climate*, *22*(15), 4162-4181.

Mölg, T., Rott, H., Kaser, G., Fischer, A., & Cullen, N. J. (2006). Comment on "Recent glacial recession in the Rwenzori Mountains of East Africa due to rising air temperature" by Richard G. Taylor et al. za. *Geophysical Research Letters*, *33*(20).

Moron, V., Robertson, A.W., Ward, M.N., & Camberlin, P. (2007). Spatial Coherence of tropical rainfall at Regional Scale. *J Climate* 20: 5244-5263.

Moron, V., Camberlin, P., & Robertson, A. W. (2013). Extracting subseasonal scenarios: an alternative method to analyze seasonal predictability of regional-scale tropical rainfall. *Journal of Climate*, *26*(8), 2580-2600.

Muchiri, P. (2007). Climate of Somalia, FAO-SWALIM. *Kenya, Nairobi*.

Mukabana, J.R., & Pielke, R.A. (1996). Investigating the influence of synoptic-scale monsoonal winds and mesoscale circulations on diurnal weather patterns over Kenya using a mesoscale numerical model. *Mon. Wea. Rev*., 124, 224-243.

Müller, R., Pfeifroth, U., Träger-Chatterjee, C., Cremer, R., Trentmann, J., & Hollmann, R. (2015). Surface Solar Radiation Data Set - Heliosat (SARAH) - Edition 1. Satellite Application Facility on Climate Monitoring. DOI:10.5676/EUM_SAF_CM/SARAH/V001. http://dx.doi.org/10.5676/EUM_SAF_CM/SARAH/V001

Mutai, C.C., & Ward, M. N. (2000). East African rainfall and the tropical circulation / convection on intraseasonal to interannual timescales. *Journal of Climate* 13: 3915-3939.

Mutai, C., Polzin, D. & Hastenrath, S. (2012). Diagnosing Kenya Rainfall in Boreal Autumn: Further Exploration. *J. Climate*, **25**, 4323–4329

Nakamura, K. (1968). Equatorial westerlies over East Africa and their climatological significance. Geogr. Rep. 3:43–61, Tokyo Metropolitan University.

Nganga, J. K.,& Masumba, B. A. N. (1988). The land and sea breeze circulation and its influence on rainfall over Kenya's coastal areas. *WMO, T.M.R.P. Report Series* **28**, 220–221.

Nicholson, S. E. (1996). A review of climate dynamics and climate variability in Eastern Africa. In *The limnology, climatology and paleoclimatology of the east african lakes,* Johnson T.C. & Odada E.O., Eds. Gordon and Breach, 25-56.

Nicholson, S.E., & Yin, X. (2002). Mesoscale patterns of rainfall, cloudiness and evaporation over the Great Lakes of Africa. In *The East African Great Lakes: Limnology, Palaeolimnology and Biodiversity*. E.O. Odada & D. O. Olago, eds. Kluwer Academic Publishers, Dordrecht, Netherlands, 93-120.

Nicholson, S.E. (2015a). The Turkana low-level jet: mean climatology and association with regional aridity. *International Journal of Climatology*. doi:10.1002/joc.4515

Nicholson, S.E. (2015b). The Predictability of Rainfall over the Greater Horn of Africa. Part II: Prediction of Monthly Rainfall during the Long Rains. *Journal of Hydrometeorology*, *16*(5), 2001-2012.

Nicholson, S.E. (2015c). Long-term variability of the East African 'short rains' and its links to large-scale factors. *International Journal of Climatology* **35**:10.1002/joc.2015.35.issue-13, 3979-3990

Nieuwolt, S. (1974). Rainstorm distributions in Tanzania. *Geografiska Annaler. Series A. Physical Geography*, 241-250.

Obasi, G.O.P. (1977). Forecasting techniques in East Africa. WMO, Technical Publication n°492, 126-150.

Ogallo, L. J. (1988). Relationships between seasonal rainfall in East Africa and the Southern Oscillation. *Journal of Climatology* 8: 31-43.

Ogallo, L.J. (1989). The spatial and temporal patterns of the East African seasonal rainfall derived from principal component analysis. *J Climatol* 9: 145-167.

Ogallo, L. J., Janowiak, J. E., & Halpert, M. S. (1988). Teleconnection between seasonal rainfall over East Africa and global sea surface temperature anomalies. *Journal of the Meteorological Society of Japan*, *66*(6), 807-822.

Okoola, R.E. (1980). The Nairobi heat-island. *Kenya Journal of Science and Technology*, Series A, 1, 53–61.

Okoola, R.E. (1989). Westwards moving disturbances in the Southwest Indian Ocean. *Met. Atmos. Phys.*, 41, 35-44.

Okoola, R.E. (1990). The stability of the South-East monsoons and the associated non-precipitating stratocumulus clouds over Eastern Africa. In Third WMO Symposium on meteorological aspects of Tropical Droughts, Niamey, 30 Apr.- 4 May 1990, WMO *Trop. Met. Res. Project Report*, 36, 65-70.

Okoola, R.E. (1999). A diagnostic study of the Eastern Africa Monsoon circulation during the Northern Hemisphere spring season. *Int. J. Climatol.*, **19,** 143–168.

Omeny, P. A., Ogallo, L., Okoola, R., Hendon, H., & Wheeler, M. (2008). East African rainfall variability associated with the Madden-Julian Oscillation. *Journal of Kenya Meteorological Society*, *2*, 2, 105-114.

Omondi, P. A. O., Awange, J. L., Forootan, E., Ogallo, L. A., Barakiza, R., Girmaw, G. B., ... & Kilavi, M. (2014). Changes in temperature and precipitation extremes over the Greater Horn of Africa region from 1961 to 2010. *International Journal of Climatology*, *34*(4), 1262-1277.

Osman, O. E., & Hastenrath, S. (1969). On the synoptic climatology of summer rainfall over Central Sudan. *Archiv für Meteorologie, Geophysik und Bioklimatologie*, Ser. B, 17: 297-324.

Osman, Y. Z., & Shamseldin, A. Y. (2002). Qualitative rainfall prediction models for central and southern Sudan using El Niño-southern oscillation and Indian Ocean sea surface temperature Indices. *International Journal of Climatology* 22 (15): 1861-1878

Otieno, V. O., & Anyah, R. O. (2012). Effects of land use changes on climate in the Greater Horn of Africa. *Climate Research*, *2*, 77.

Ozer, P., & Mahamoud, A. (2013). Recent extreme precipitation and temperature changes in Djibouti city (1966–2011). *Journal of Climatology*, doi:10.1155/2013/928501.

Peagle, J., & Geisler, J.E. (1986). The effect of East African topography on flow driven by zonally symmetric forcing. *J Atmos. Sc*., 43, 17, 1862-1872.

Pedgley, D.E., (1966). The Red Sea convergence zone. *Weather*, 21. 350-358 et 394-406.

Pedgley, D. E. (1967). Air temperature at Dallol, Ethiopia. *Meteorological Magazine*, *96*(1142), 265.

Pedgley, D. E. (1969). Diurnal variation of the incidence of monsoon rainfall over the Sudan. *Meteorological Magazine* 98: 97-106 & 129-134.

Pepin, N. C., Duane, W. J., Schaefer, M., Pike, G., & Hardy, D. R. (2014). Measuring and modeling the retreat of the summit ice fields on Kilimanjaro, East Africa. *Arctic, Antarctic, and Alpine Research*, *46*(4), 905-917.

Philipps, J., & McIntyre, B. (2000). ENSO and interannual rainfall variability in Uganda: implications for agricultural management. *International Journal of Climatology* 20 (2): 171-182.

Pohl, B., & Camberlin, P. (2006a). Influence of the Madden-Julian Oscillation on East African rainfall. Part I: Intraseasonal variability and regional dependency. *Quarterly Journal of the Royal Meteorological Society* 132(621): 2521-2539.

Pohl, B., & Camberlin, P. (2006b). Influence of the Madden–Julian Oscillation on East African rainfall: II. March–May season extremes and interannual variability. *Quarterly Journal of the Royal Meteorological Society*, *132*(621), 2541-2558.

Price, C., Yair, Y., & Asfur, M. (2007). East African lightning as a precursor of Atlantic hurricane activity. *Geophysical research letters*, *34*(9). doi:1029/2006GL028884.

Riddle, E. E., & Cook, K. H. (2008). Abrupt rainfall transitions over the Greater Horn of Africa: Observations and regional model simulations. *Journal of Geophysical Research: Atmospheres*, *113*(D15).

Riddle, E. E., & Wilks, D. S. (2013). Statistical indices of the northward rainfall progression over eastern Africa. *International Journal of Climatology*, *33*(2), 356-375.

Rohde, R., Muller, R., Jacobsen, R., Perlmutter, S., Rosenfeld, A., Wurtele, J., ... & Mosher, S. (2013). Berkeley earth temperature averaging process. *Geoinfor Geostat: An Overview*, *1*(2), 1-13.

Røhr, P. C., & Killingtveit, Å. (2003). Rainfall distribution on the slopes of Mt Kilimanjaro. *Hydrological sciences journal*, *48*(1), 65-77.

Rosell, S. (2011). Regional perspective on rainfall change and variability in the central highlands of Ethiopia, 1978–2007. *Applied Geography*, *31*(1), 329-338.

Rowell, D. P., Booth, B. B., Nicholson, S. E., & Good, P. (2015). Reconciling past and future rainfall trends over east Africa. *Journal of Climate*, *28*(24), 9768-9788.

Saji, N. H., Goswami, B. N., Vinayachandran, P. N., & Yamagata, T. (1999). A dipole mode in the tropical Indian Ocean. *Nature*, *401*(6751), 360-363.

Sansom, H.W. (1966). Occurence and distribution of hail in Africa. Meteorological Magazine, 95,212-218.

Savijärvi, H. (1997). Diurnal winds around Lake Tanganyika. *Quarterly Journal of the Royal Meteorological Society*, *123*(540), 901-918.

Schneider, U., Becker, A., Finger, P., Meyer-Christoffer, A., Rudolf, B., & Ziese, M. (2011). GPCC Full Data Reanalysis Version 6.0 at 0.5°: Monthly Land-Surface Precipitation from Rain-Gauges built on GTS-based and Historic Data. DOI: 10.5676/DWD_GPCC/FD_M_V7_050

Segele, Z.T., Lamb, P.J., Leslie, L.M. (2009). Large-scale atmospheric circulation and global sea surface temperature associations with Horn of Africa June-September rainfall. *International Journal of Climatology* 29(8): 1075-1100.

Seleshi, Y., Demarée, G. R. (1995). Rainfall variability in the Ethiopian and Eritrean highlands and its links with the Southern Oscillation Index. *Journal of Biogeography*, 22: 945-952.

Shamseddin, M. A. H., Hata, T., Tada, A., Bashir, M. A., & Tanakamaru, T. (2006). Estimation of flooded area in the Bahr El-Jebel basin using remote sensing techniques. *Hydrology and Earth System Sciences Discussions*, *3*(4), 1851-1877.

Sissons, J. (1966). Some examples of synoptic situations which affect East Africa. *Weather*, 21, 228-231; 260-262; 298-300.

Slingo, J., Spencer, H., Hoskins, B., Berrisford, P., & Black, E. (2005). The meteorology of the Western Indian Ocean, and the influence of the East African Highlands. *Philosophical Transactions of the Royal Society of London A: Mathematical, Physical and Engineering Sciences*, *363*(1826), 25-42.

Song, Y., Semazzi, F. H., Xie, L., & Ogallo, L. J. (2004). A coupled regional climate model for the Lake Victoria basin of East Africa. *International Journal of Climatology*, *24*(1), 57-75.

Stephens, W., Othieno, C. O., & Carr, M. K. V. (1992). Climate and weather variability at the Tea Research Foundation of Kenya. *Agricultural and forest meteorology*, *61*(3), 219-235.

Sumner, G. N. (1982). Rainfall and wind circulation in Coastal Tanzania. *Archives for meteorology, geophysics, and bioclimatology, Series B*, *30*(1-2), 107-125.

Sumner, G. N. (1983). Daily rainfall variability in coastal Tanzania. *Geografiska Annaler. Series A. Physical Geography*, 53-66.

Sumner, G. N. (1984). The impact of wind circulation on the incidence and nature of rainstorms over Dar es Salaam, Tanzania. *Journal of climatology*, *4*(1), 35-52.

Sun, L., Semazzi, F. H., Giorgi, F., & Ogallo, L. (1999). Application of the NCAR regional climate model to eastern Africa: 1. Simulation of the short rains of 1988. *Journal of Geophysical Research: Atmospheres*, *104*(D6), 6529-6548.

Süring, R., 1910: A. Berson's Bericht über die aerologische Expedition des königlichen aeronautischen Observatoriums nach Ostafrika im Jahre 1908. - *Meteorol. Z.* 27, 536–542.

Sutcliffe, J. V., & Parks, Y. P. (1999). *The hydrology of the Nile* (No. 5). Wallingford, Oxfordshire, UK: International Association of Hydrological Sciences.

Taylor, R.G., Mileham, L., Tindimugaya, C., Majugu, A., Nakileza, R., & Muwanga, A. (2006). Recent deglaciation in the Rwenzori Mountains of East Africa due to rising air temperatures. *Geophysical Research Letters* Vol. 33, L10402.

Thiery, W., Davin, E. L., Panitz, H. J., Demuzere, M., Lhermitte, S., & Van Lipzig, N. (2015). The impact of the African Great Lakes on the regional climate. *Journal of Climate*, *28*(10), 4061-4085.

Thompson, B.W. (1966). The mean annual rainfall of Mount Kenya. *Weather*, 21, 48-49.

Thompson, L. G., Brecher, H. H., Mosley-Thompson, E., Hardy, D. R., & Mark, B. G. (2009). Glacier loss on Kilimanjaro continues unabated. *Proceedings of the National Academy of Sciences*, *106*(47), 19770-19775.

Thompson, L.G., Mosley-Thompson, E., Davis, M.E., Henderson, K.A., Brecher, H.H., Zagorodnov, V.S., Mashiotta, T.A., Lin, P.-N., Mikhalneko, V.N., Hardy, D.R., & Beer, R. (2002). Kilimanjaro ice core records: evidence of Holocene climate change in tropical Africa. *Science* 298, 589-593.

Tomsett, J. E. (1975). The diurnal variation of precipitation in East Africa. East African Meteorological Department, Nairobi, Technical Memorandum n° 25, 66 pp.

Trewartha, G. T. (1961). *The earth's problem climates*. University of Wisconsin Press.

Tucker, M. R., & Pedgley, M. D. (1977). Summer winds around the southern Red Sea. *Archiv für Meteorologie, Geophysik und Bioklimatologie, Serie B*, *25*(3), 221-231.

Ummenhofer, C. C., Sen Gupta, A., England, M. H., & Reason, C. J. (2009). Contributions of Indian Ocean sea surface temperatures to enhanced East African rainfall. *Journal of Climate*, *22*(4), 993-1013.

UNDP/UNSO (1997). *Aridity zones and dryland populations: An assessment of population levels in the world's drylands with particular reference to Africa*. UNDP Office to Combat Desertification and Drought (UNSO), New York.

UNEP (2010). *Africa Water Atlas*. United Nations Environment Programme / Earthprint.

United Nations (2015). *World Urbanization Prospects: The 2014 Revision*. UN Department of Economic and Social Affairs, Population Division.

Viste, E., & Sorteberg, A. (2013). Moisture transport into the Ethiopian highlands. *International journal of climatology*, *33*(1), 249-263.

Viste, E., Korecha, D., & Sorteberg, A. (2013). Recent drought and precipitation tendencies in Ethiopia. *Theoretical and Applied Climatology*, *112*(3-4), 535-551.

Wheeler, M. C., & Hendon, H. H. (2004). An all-season real-time multivariate MJO index: Development of an index for monitoring and prediction. *Monthly Weather Review*, *132*(8), 1917-1932.

Williams, A., & Funk, C. (2011). A westward extension of the warm pool leads to a westward extension of the Walker circulation, drying eastern Africa. *Climate Dynamics*, 37, (11) 2417 – 2435, DOI:10.1007/s00382-010-0984-y.

Williams, A. P., Funk, C., Michaelsen, J., Rauscher, S. A., Robertson, I., Wils, T. H., ... & Loader, N. J. (2012). Recent summer precipitation trends in the Greater Horn of Africa and the emerging role of Indian Ocean sea surface temperature. *Climate Dynamics*, *39*(9-10), 2307-2328.

Williamson, D., Majule, A., Delalande, M., Mwakisunga, B., Mathé, P. E., Gwambene, B., & Bergonzini, L. (2014). A potential feedback between landuse and climate in the Rungwe tropical highland stresses a critical environmental research challenge. *Current opinion in environmental sustainability*, *6*, 116-122.

Yang, W., Seager, R., Cane, M. A., & Lyon, B. (2015). The annual cycle of east African precipitation. *Journal of Climate*, *28*(6), 2385-2404.

Yin, X., & Nicholson, S.E. (1998). The water balance of Lake Victoria. *Hydrol. Sc. J.*, 43 (5), 789-811.

Zaroug, M. A., Sylla, M. B., Giorgi, F., Eltahir, E. A., & Aggarwal, P. K. (2013). A sensitivity study on the role of the swamps of southern Sudan in the summer climate of North Africa using a regional climate model. Theoretical and applied climatology, 113(1-2), 63-81.

Zaroug, M. A. H., Eltahir, E. A. B., & Giorgi, F. (2014). Droughts and floods over the upper catchment of the Blue Nile and their connections to the timing of El Niño and La Niña events. *Hydrol. Earth Syst. Sci*, *18*, 1239-1249.

Zipser, E. J., Liu, C., Cecil, D. J., Nesbitt, S. W., & Yorty, D. P. (2006). Where are the most intense thunderstorms on Earth?. *Bulletin of the American Meteorological Society*, *87*(8), 1057-1071.

Zhai, P., & Bower, A. (2013). The response of the Red Sea to a strong wind jet near the Tokar Gap in summer. *Journal of Geophysical Research*, 118(1), 422-434, doi: 10.1029/2012JC008444.

Zorita, E., & Tilya, F. F. (2002). Rainfall variability in Northern Tanzania in the March-May season (long rains) and its links to large-scale climate forcing. *Climate Research*, *20*(1), 31-40.

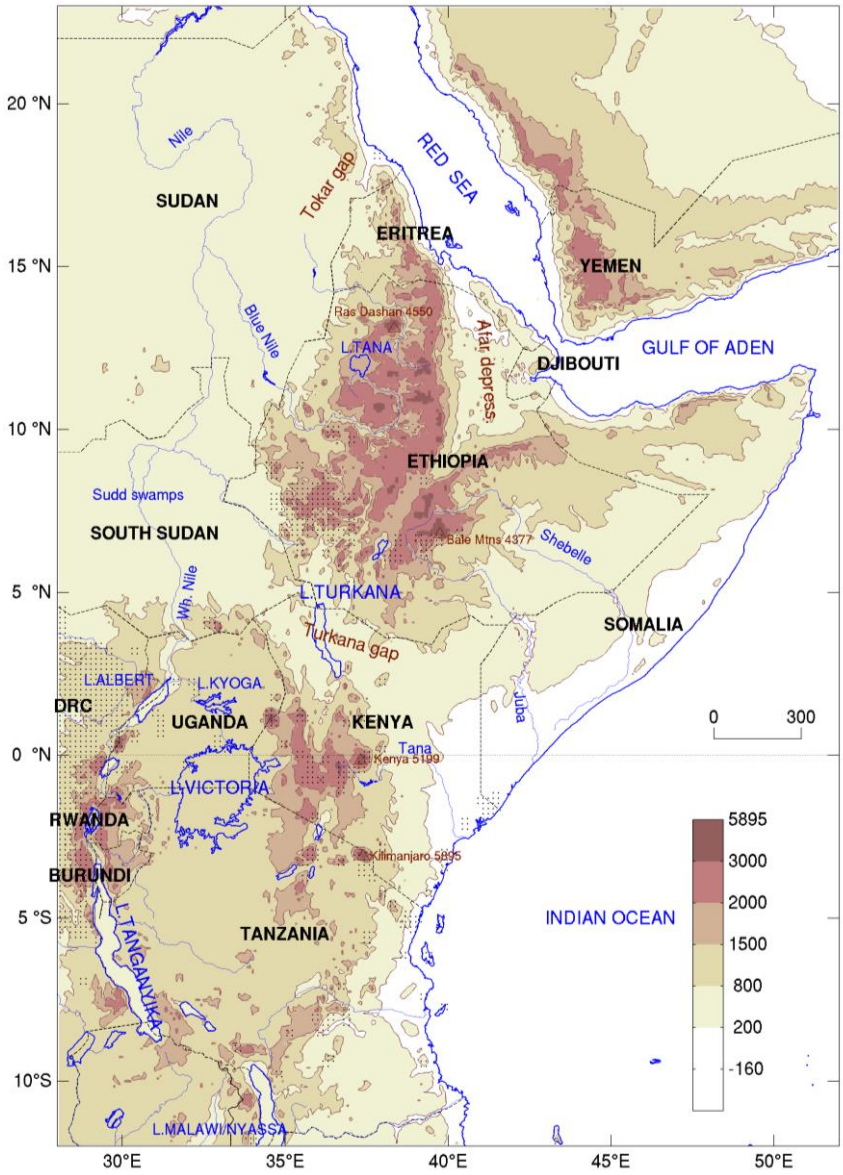

Figure 1 : Location map of eastern Africa, showing terrain (shading : altitude in meters a.m.s.l), water bodies, country boundaries and forest cover (small dotted areas : evergreen forests from GLC 2000 ; Mayaux et al., 2004)

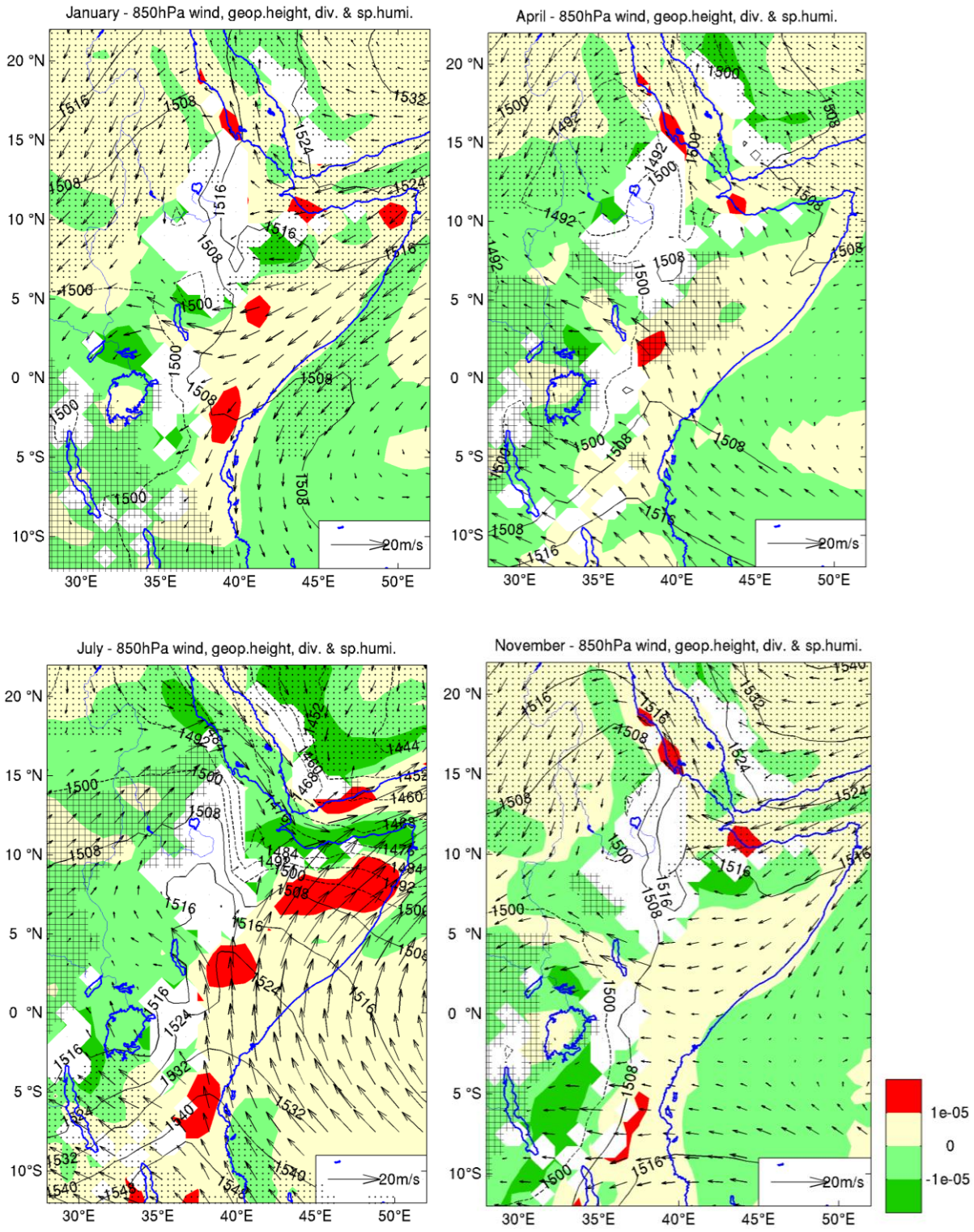

Figure 2 : 850 hPa mean monthly winds (vectors), geopotential height (contours in meters) and divergence (color shading in s^{-1}). Dots show areas where 850 hPa specific humidity is below 8 $g.kg^{-1}$, and cross-hatching areas where it is above 13 $g.kg^{-1}$. Data : ERA-interim, 1979-2014 average.

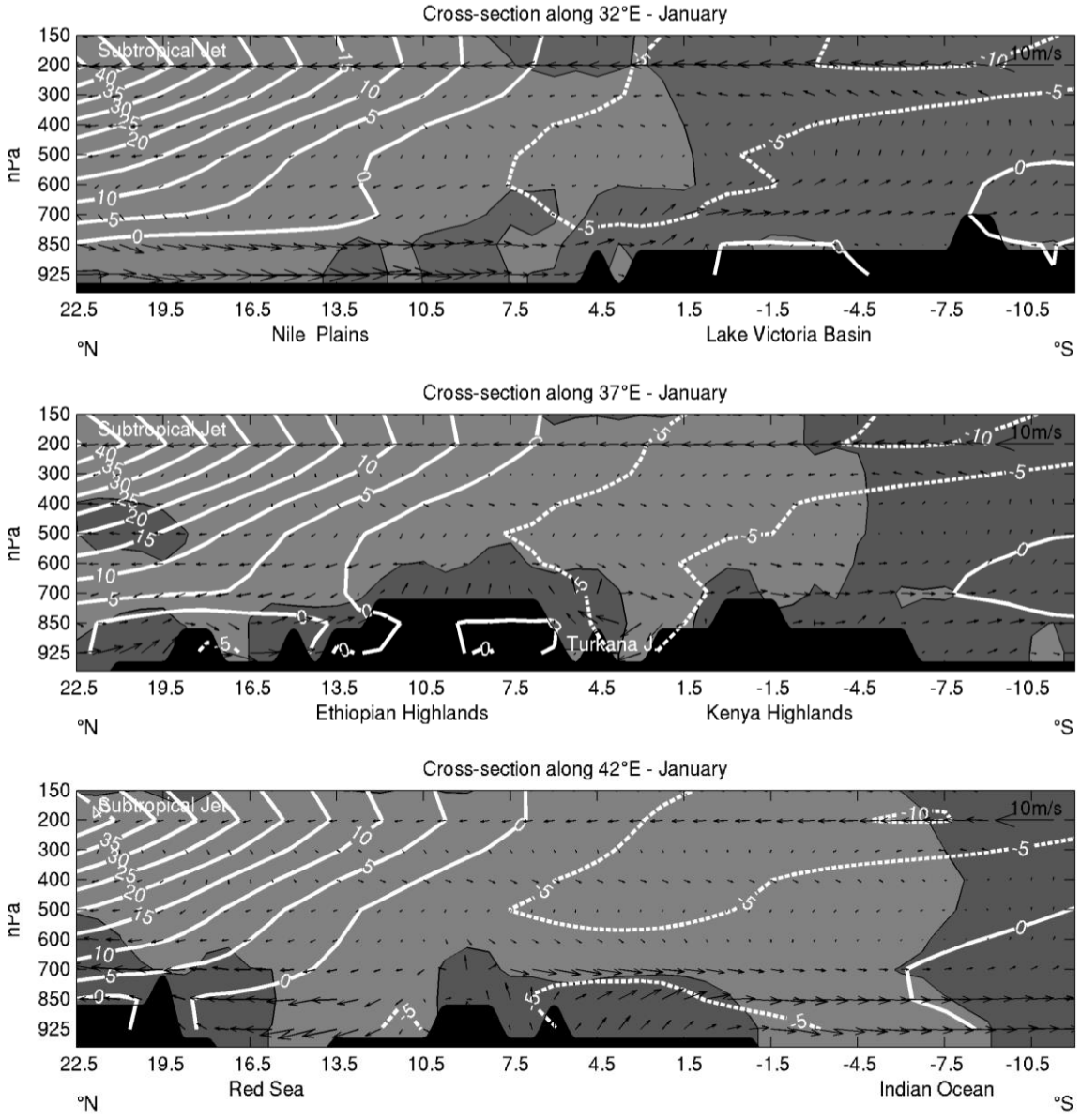

Figure 3a : North-south atmospheric cross-sections over eastern Africa for January. Vectors show meridional wind and vertical motion (with dark shading emphasizing ascending motion and light shading descending motion). White contours show zonal wind (positive values : westerlies ; negative values : easterlies). The top right vector shows the scale for meridional wind. Data : ERA-interim, 1979-2014 average.

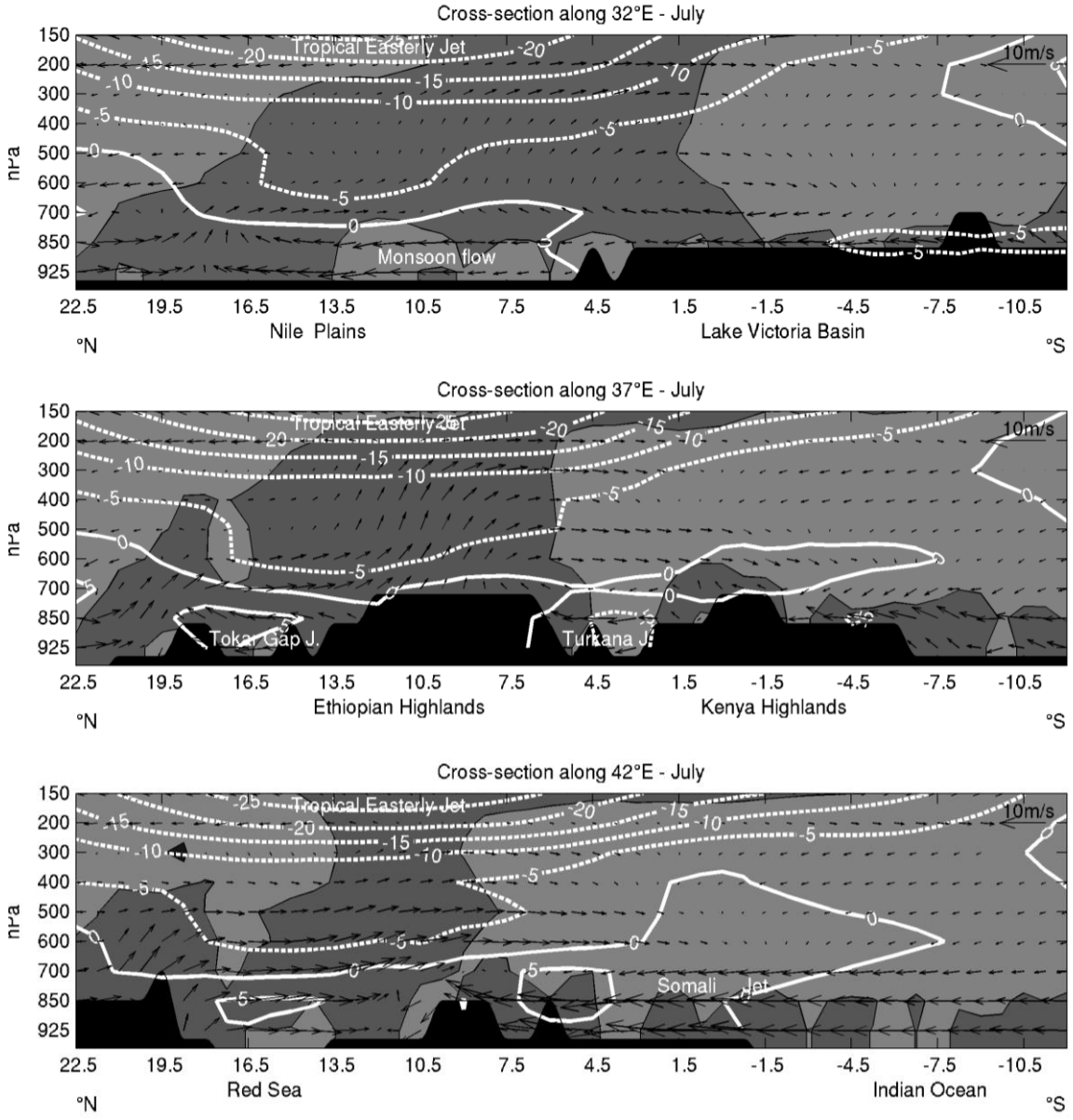

Figure 3b : North-south atmospheric cross-sections over eastern Africa for July. See legend of figure 3a.

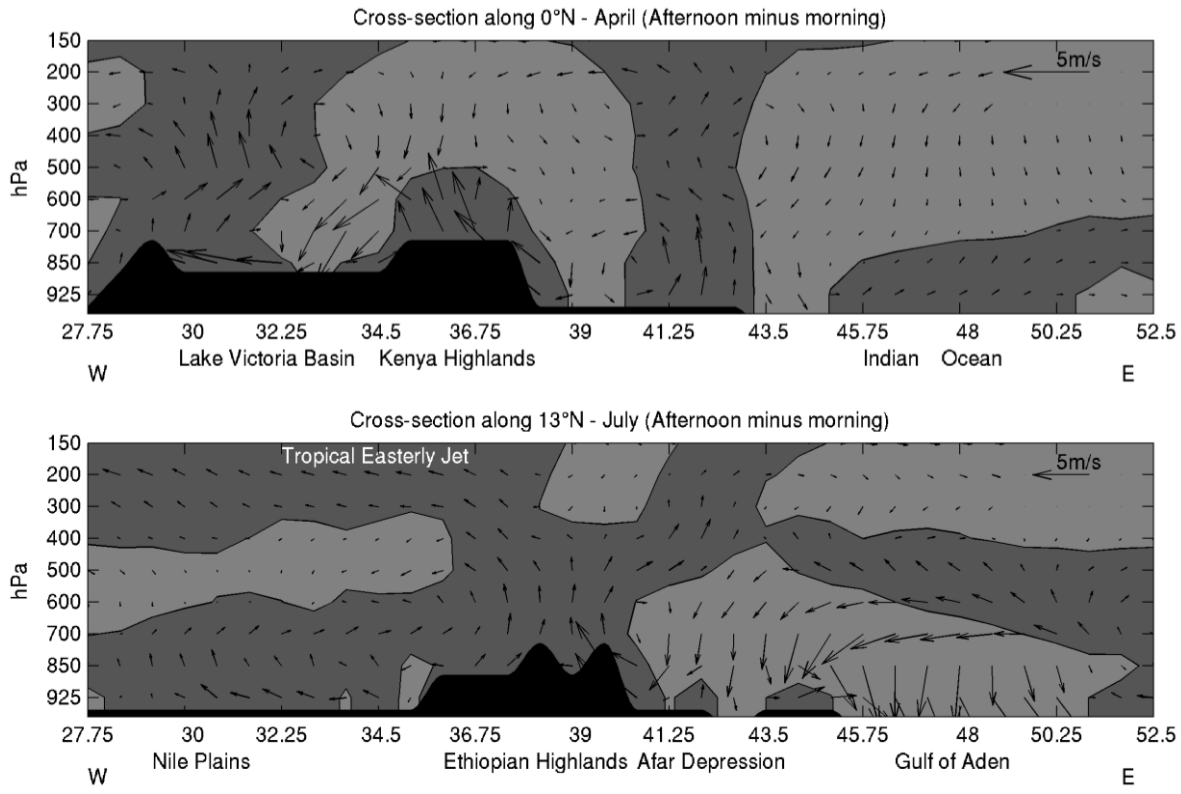

Figure 4 : Diurnal variations (1500 EAT minus 0300 EAT) of atmospheric dynamics along two west-east cross-sections (top : 0°N, April ; bottom : 13°N, July). Vectors show changes in zonal winds and vertical velocity, with dark shading indicating enhanced rising motion (or weaker descending motion) at 1500, and light shading reduced rising motion (or enhanced descending motion) at 1500. Scale for zonal wind is shown on top right corner. Data : ERA-interim 6-hourly averages, 1979-2014.

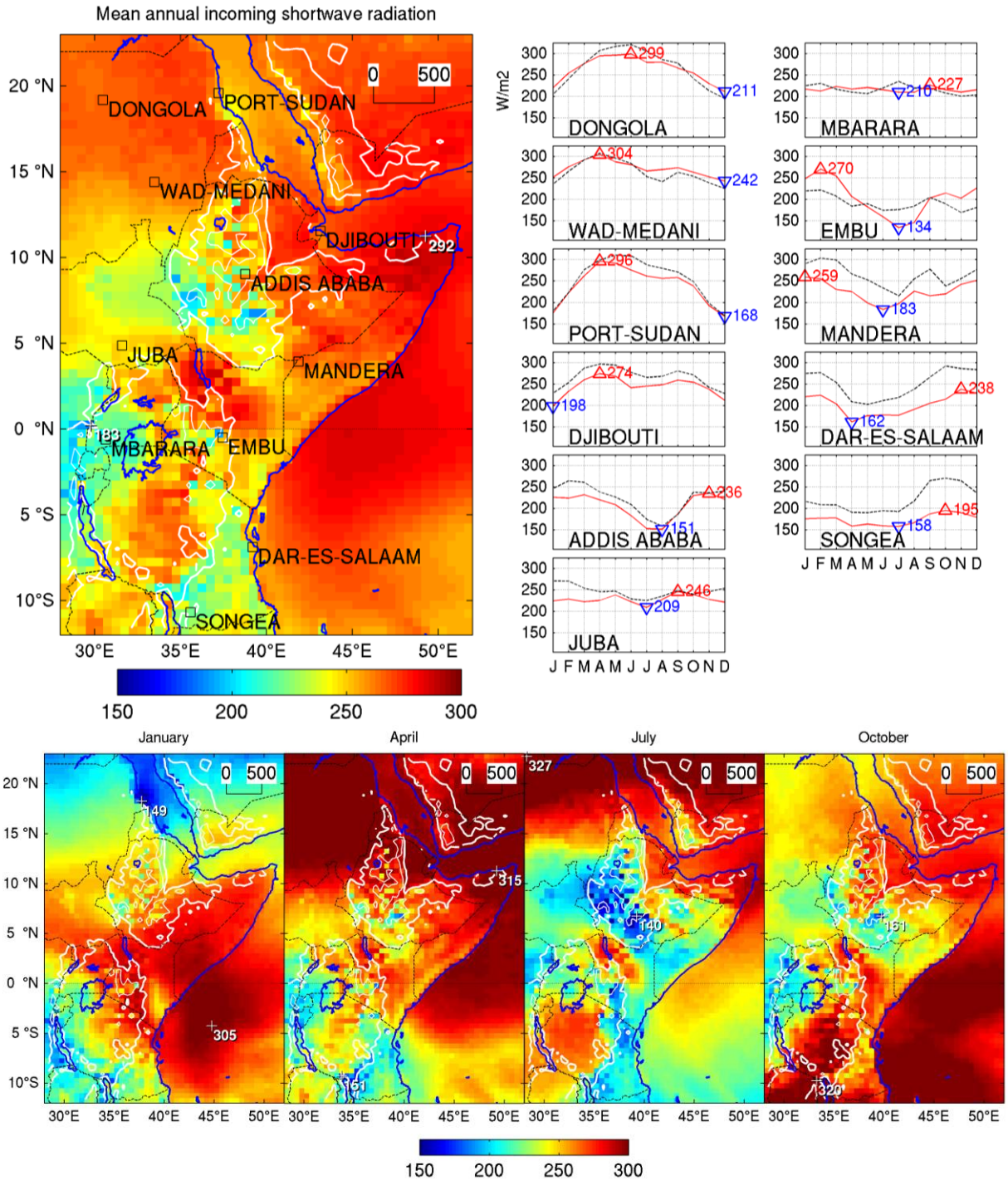

Figure 5 : Mean surface incoming shortwave solar radiation in W.m^{-2} (average for 2007-2015, MSG data from CMSAF ; Müller et al., 2015). Top left : mean annual radiation. Top right : regimes at selected locations (dotted lines : estimates from MSG data ; solid red lines : in situ measurements from World Radiation Data Centre [WRDC], based on all available data. Triangles indicate maximum and minimum values). Bottom : mean monthly radiation. White contours : 1000 m (thick lines) and 2000 m (thin lines) elevation. White figures indicate the maximum and minimum values for each plot.

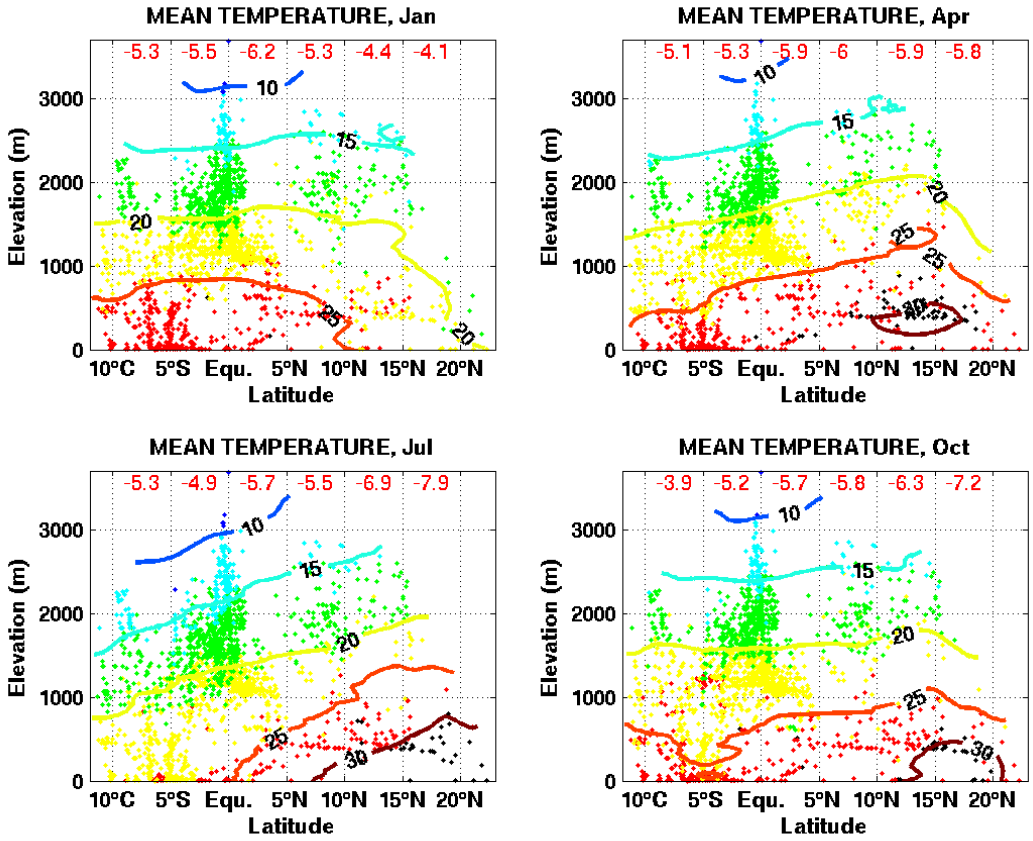

Figure 6 : Mean monthly temperature latitude-elevation plots, for 2031 stations across Eastern Africa (data : FAO agroclimatic data-base and CRC Univ. Bourgogne Franche-Comté). Contours show smoothed temperatures (°C), and top figures give lapse-rates for each 5° latitude bin.

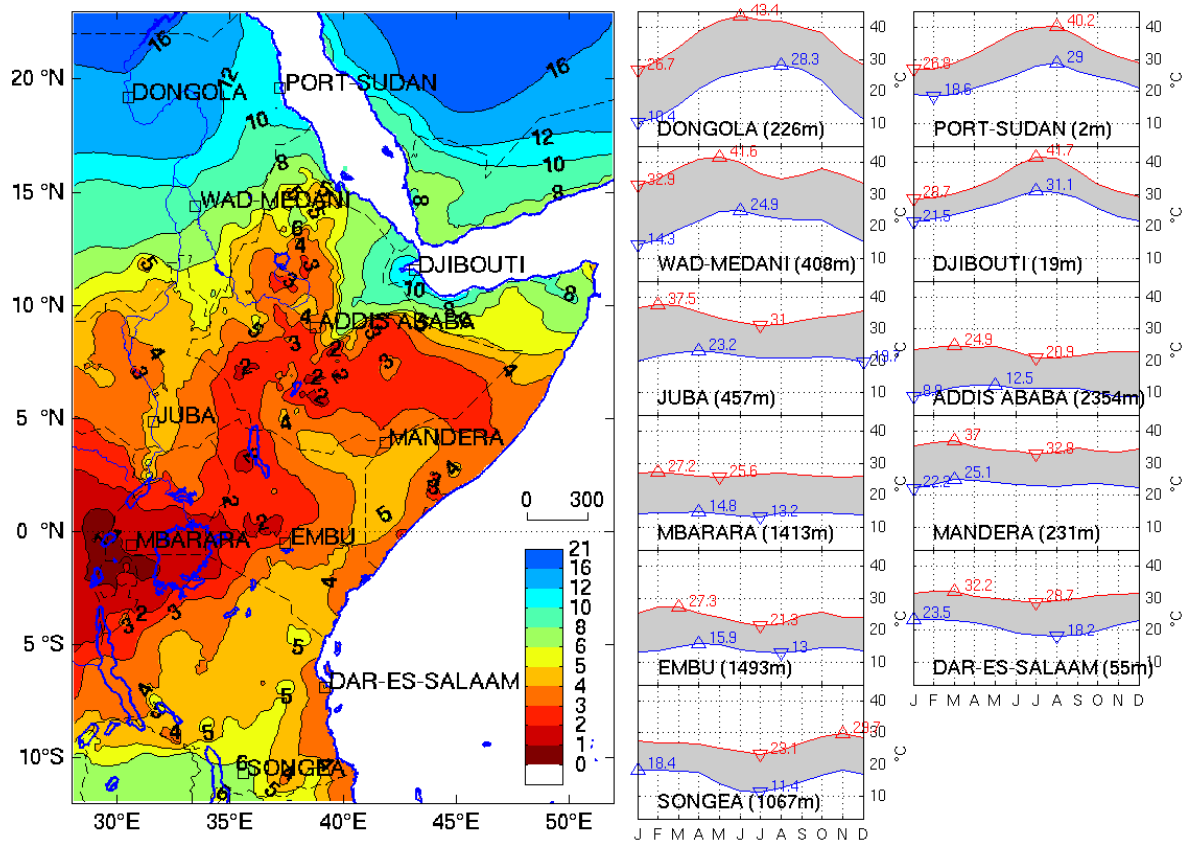

Figure 7 : Mean annual temperature range (°C, Worldclim data base, Hijmans et al. 2005). Right panels : mean monthly maximum temperature (red lines) and minimum temperature (blue lines) at selected stations (long-term averages from data covering the period 1961-2010 ; FAO and CRC data bases). Upward-pointing and downward-pointing triangles show temperatures of the warmest and coolest months, respectively (in °C).

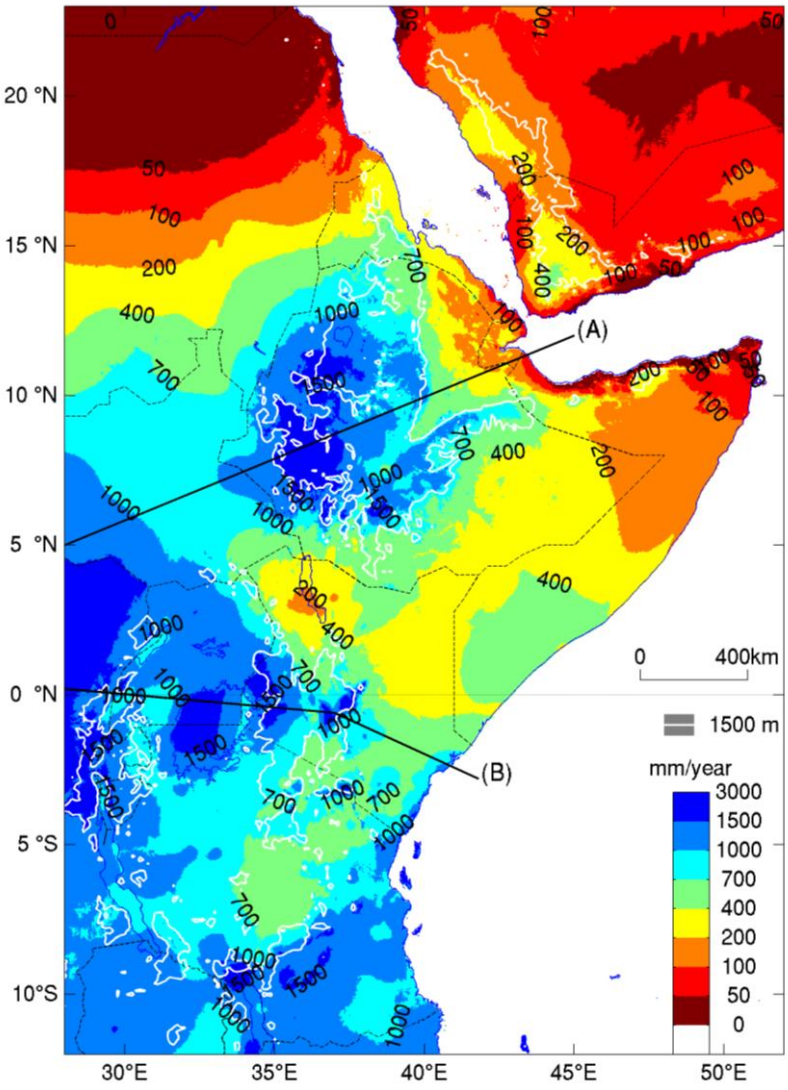

Figure 8 : Mean annual precipitation (mm) from the Worldclim data base (Hijmans et al., 2005). Thin white lines : 1500 meters a.m.s.l. contour line. Straight lines locate the transects shown in figure 9.

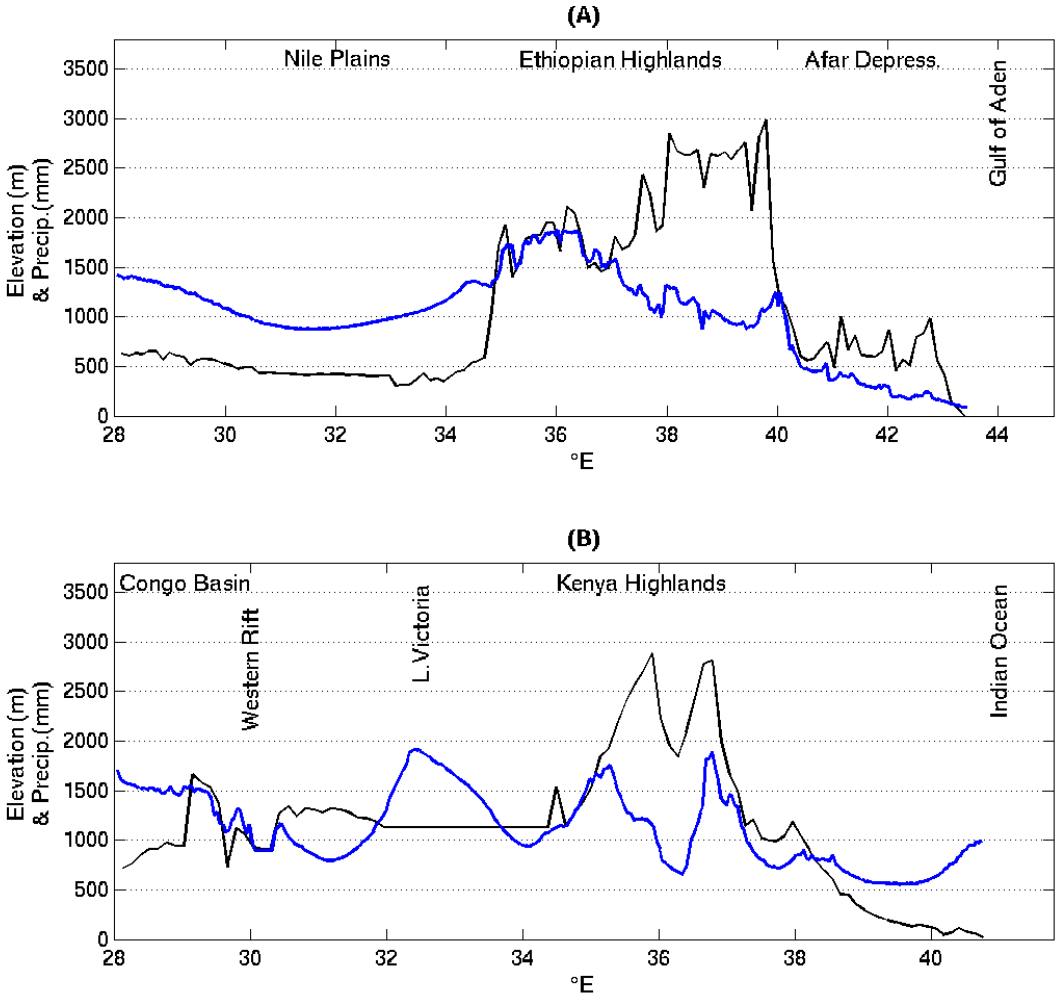

Figure 9 : Precipitation transects across eastern Africa. See figure 8 for the location of the transects. Heavy blue line : mean annual precipitation from the Worldclim data base (Hijmans et al., 2005). Light black line : altitude.

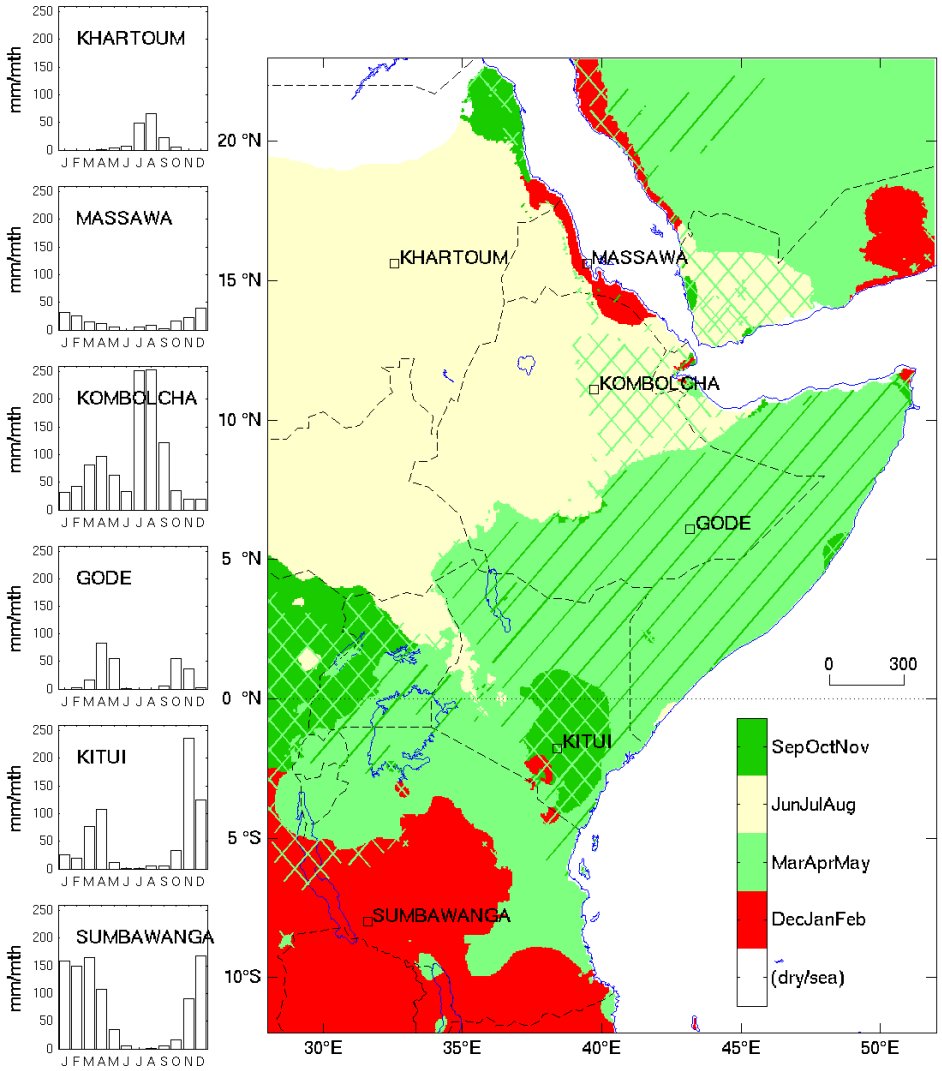

Figure 10 : Seasonal rainfall distribution over Eastern Africa. Shadings show the three-month period during which the peak rainfall month is found. Green diagonal hatching indicates a secondary peak occurring in September-November. Light green cross-hatching indicates a secondary peak in March-May. Data : Worldclim (Hijmans et al., 2005). Left panels : mean rainfall regimes at sample raingauges (all years available within the period 1951-2000, CRC data base – Univ. Bourgogne Franche-Comté).

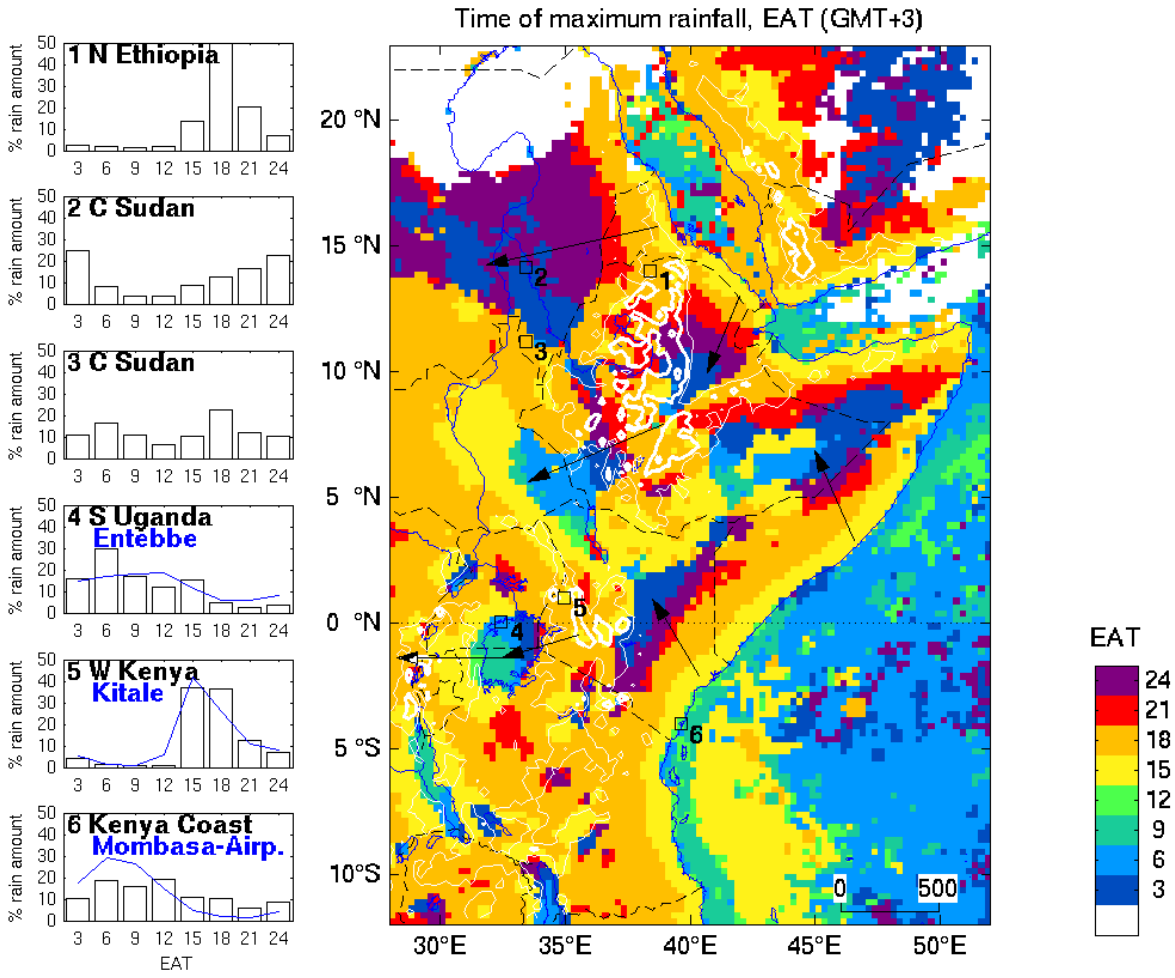

Figure 11: Diurnal rainfall regimes of eastern Africa. The map shows the local (East African Time) 3-hour period recording highest rainfall amounts (all months combined, TRMM data 1998-2014). Sample diurnal regimes for 6 locations are plotted on the left. Plots 4 to 6 correspond to the nearest grid-points to rainfall stations where local records (blue solid lines, data from Tomsett, 1975) were available. Arrows : apparent directions of dominant propagations. Thin and thick white lines show 1300 and 2200 m contour lines, respectively.

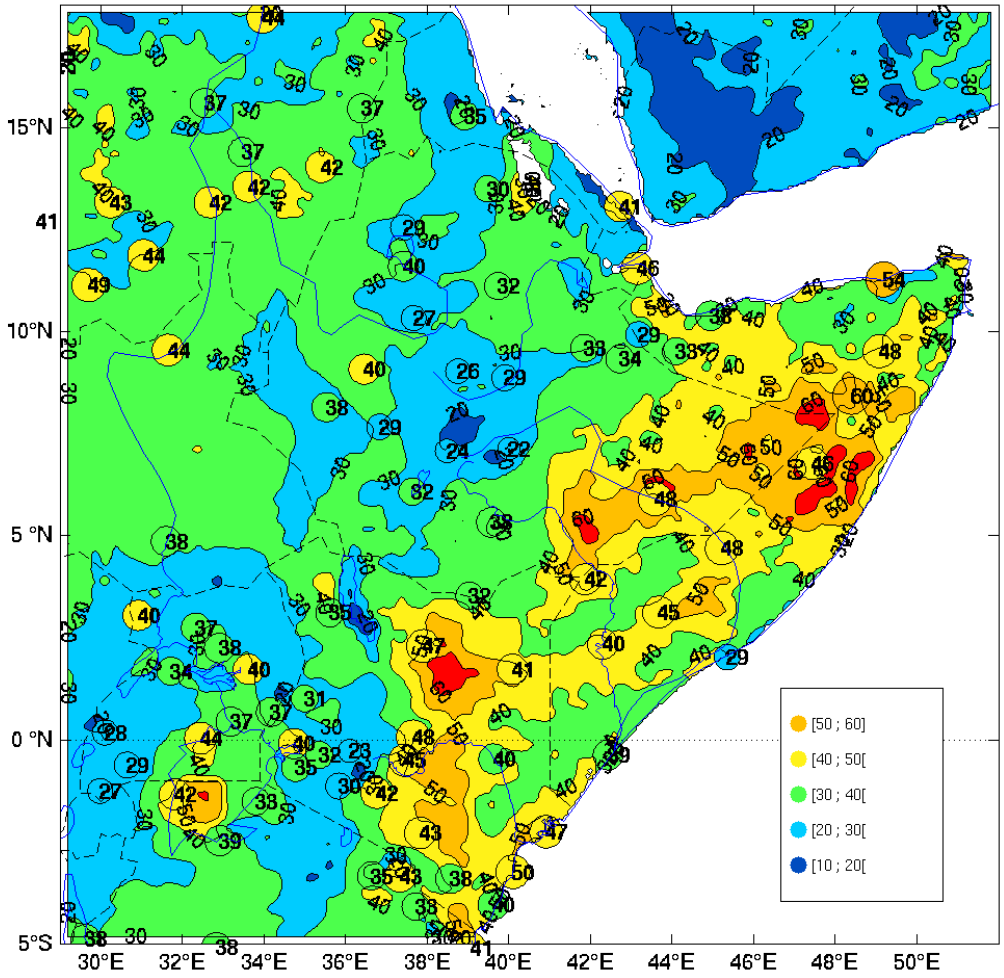

Figure 12 : Percentile 95 (P95) of daily rainfall amounts (mm) over eastern Africa. Only wet days (at least 1 mm) are considered. Shadings show P95 from TRMM data (1998-2014 ; Huffman et al. 2007). Circles with bold figures show P95 computed from daily raingauge data (CRC data base) for various periods (only stations with at least 7 years of data are retained).

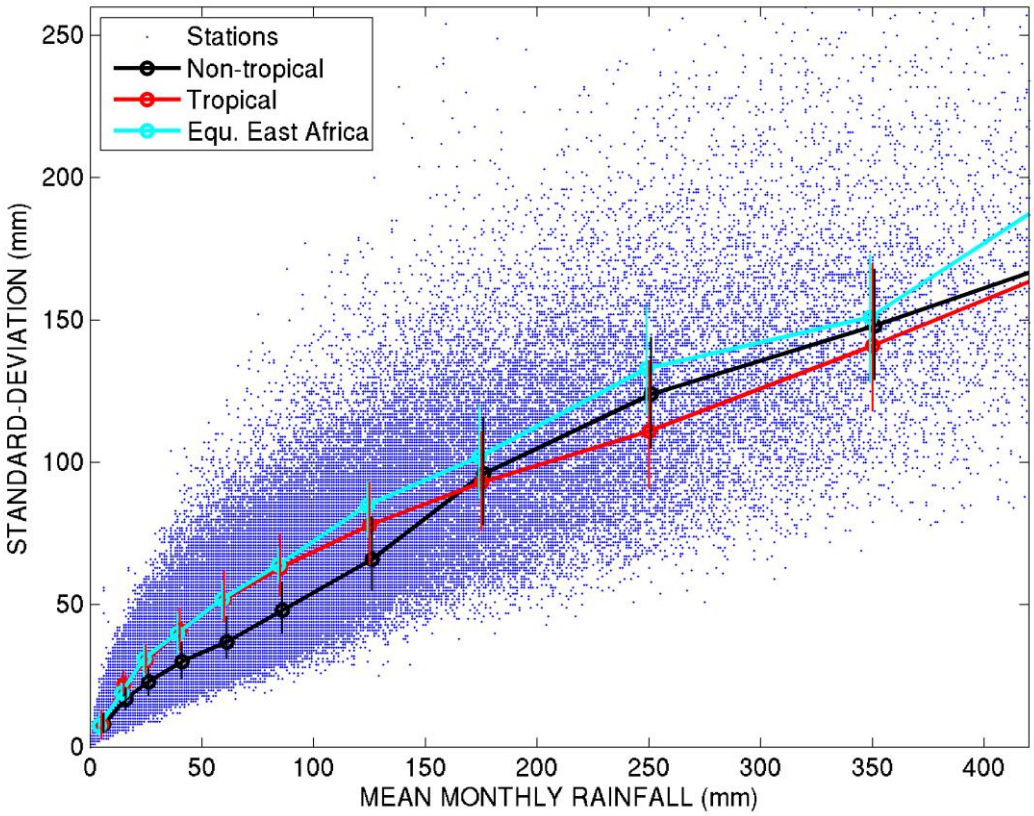

Figure 13 : Scatter-plot of monthly rainfall mean versus standard-deviation for 12347 stations over the world. Stations with at least 40 years of data over the period 1901-2005 have been used. Each dot is a given month at a given station. Black circles and lines show the median value across all non-tropical stations (latitude > 23°), red symbols across all tropical stations, and turquoise blue across stations in Equatorial East Africa only (6°S-6°N, 35-52°E). Vertical bars indicate the inter-quartile range for mean each rainfall bin. Data : GHCN-v3 (Lawrimore et al., 2011)

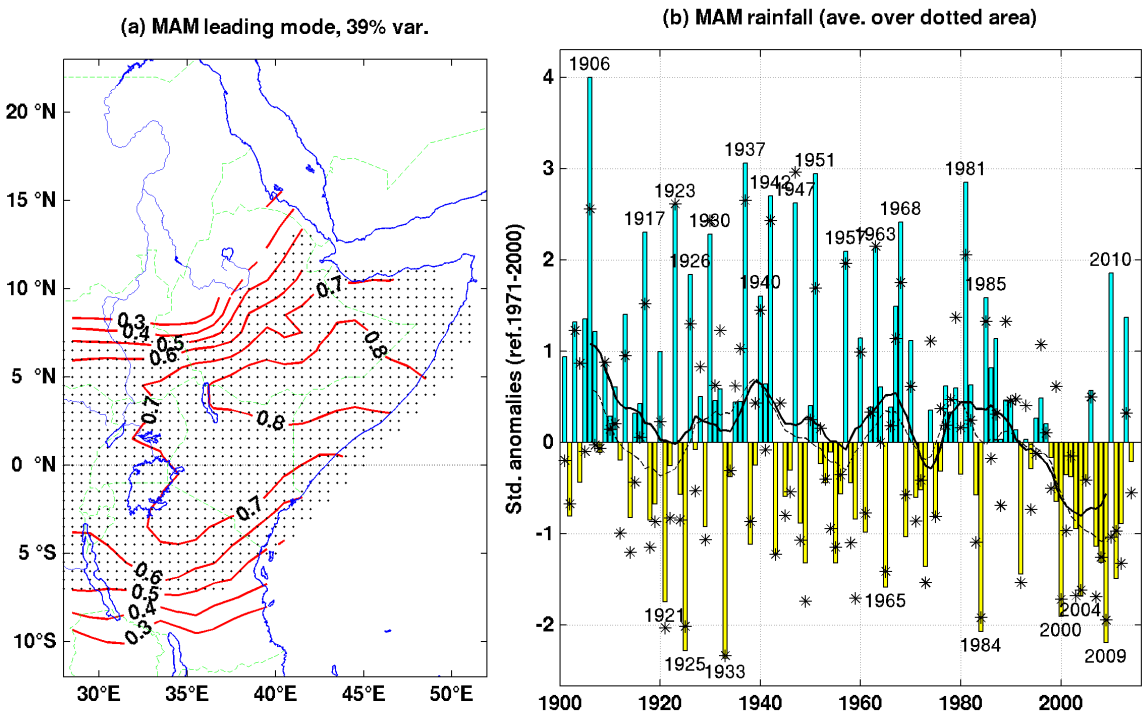

Fig.14 : Variations of March-May rainfall, 1901-2014. (a) Loading coefficients associated with the leading mode of variability (PC1 obtained from normalized time-series for all grid-points whose mean MAM rainfall exceeds 50 mm and share of annual rainfall is above 15%). The percentage of variance explained by PC1 is shown on top. Dots : grid-points correlated at >0.5 with PC1. (b) Time-series of the average rainfall for all dotted areas, standardized to the period 1971-2000. Data : CenTrends (bars) and GPCC (stars). Lines : 11-yr filtered time-series from CenTrends (solid) and GPCC data (dashed).

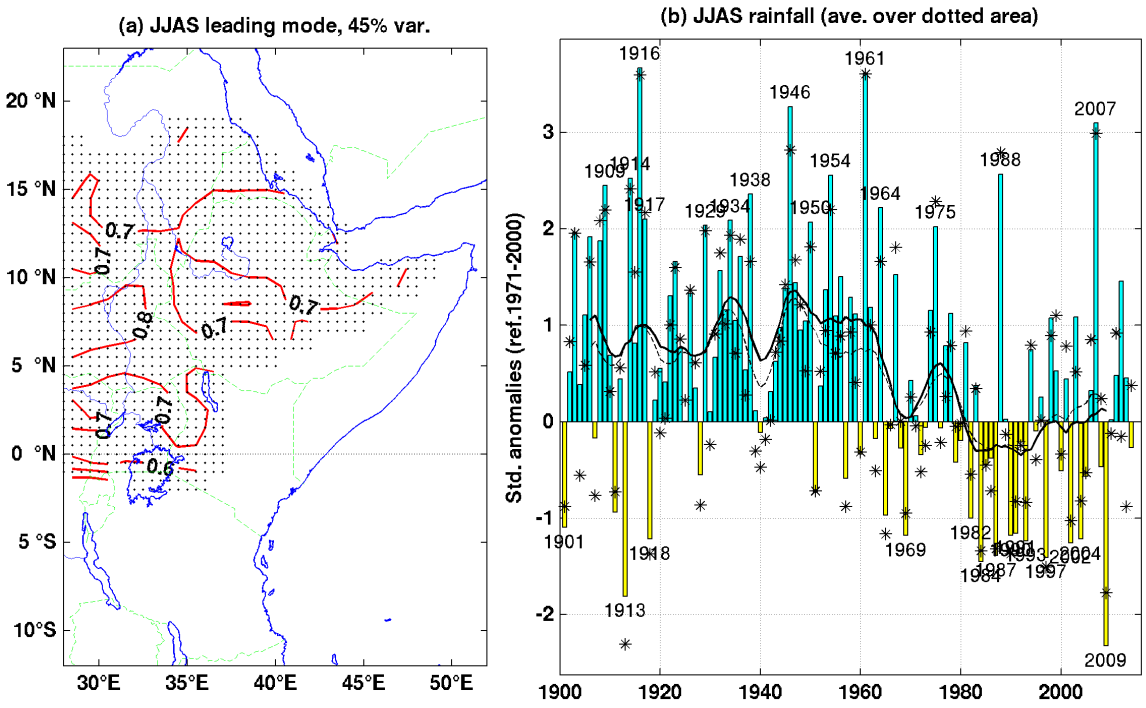

Fig.15 : Same as figure 14 but for variations of June-September rainfall, 1901-2014

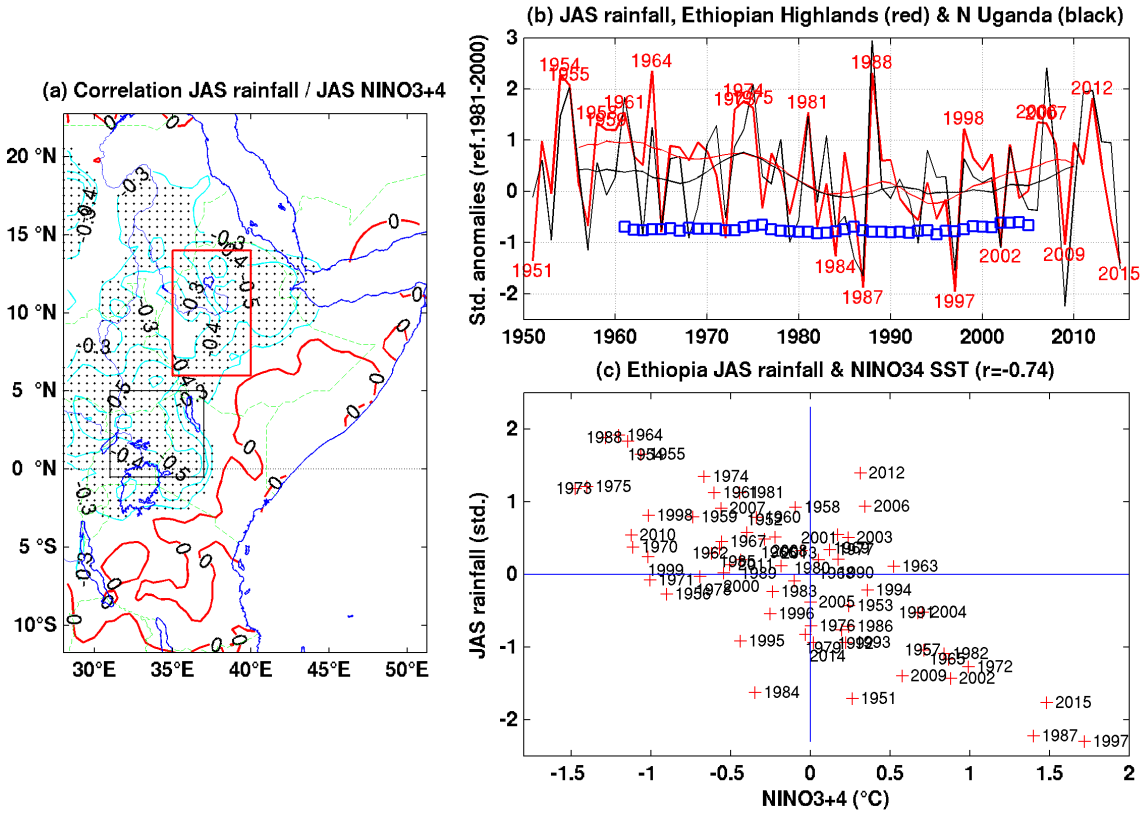

Fig.16 : Relationship between July-September rainfall and the Nino 3+4 sea surface temperature index. Rainfall data combined from CRC (1951-2000) and CHIRPS (1981-2015, Funk et al. 2015b), normalized on the period 1981-2000. (a) Correlation coefficients (1951-2015). Dots denote 99.9% significance. (b) Time-series of standardized rainfall averaged for the Ethiopian Highlands (red box in panel a), shown as red line, and Northern Uganda / Western Kenya (black box), shown as black line. Major wet and dry years in Ethiopia are indicated, and the smoothed lines are 11-yr moving averages. Blue squares are 21-yr moving correlation coefficients between Ethiopia rainfall and Nino 3+4. (c) Scatter-plot of Ethiopia rainfall vs Nino 3+4.

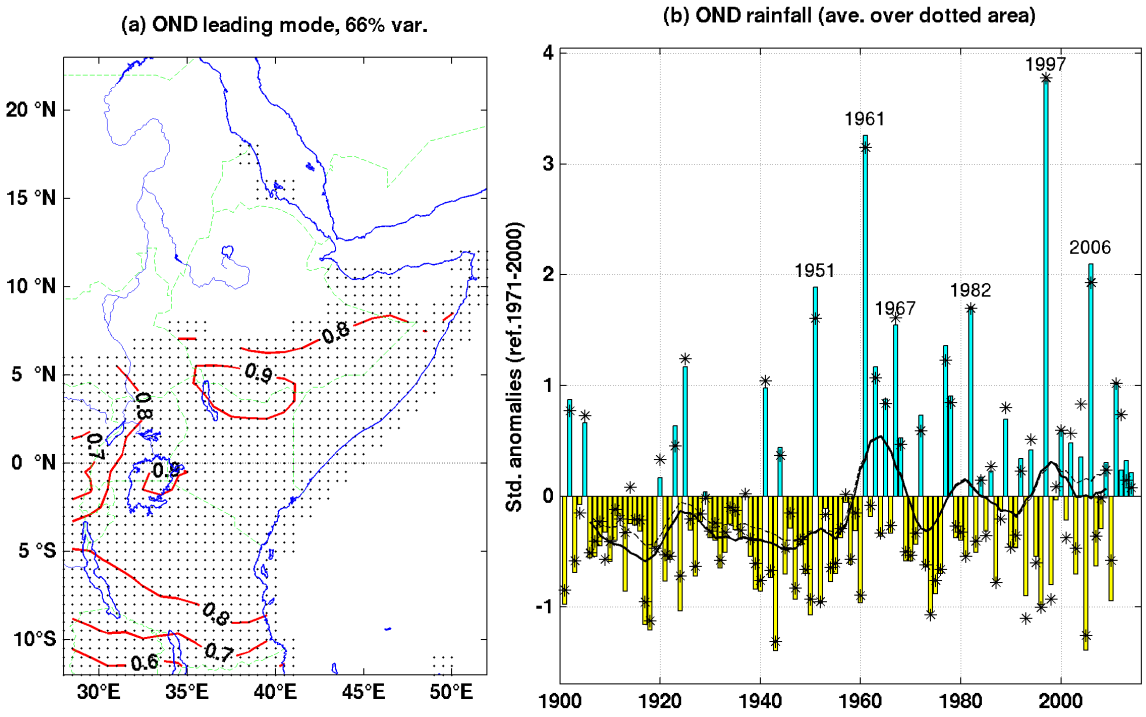

Fig.17 : Same as figure 14 but for variations of October-December rainfall, 1901-2014

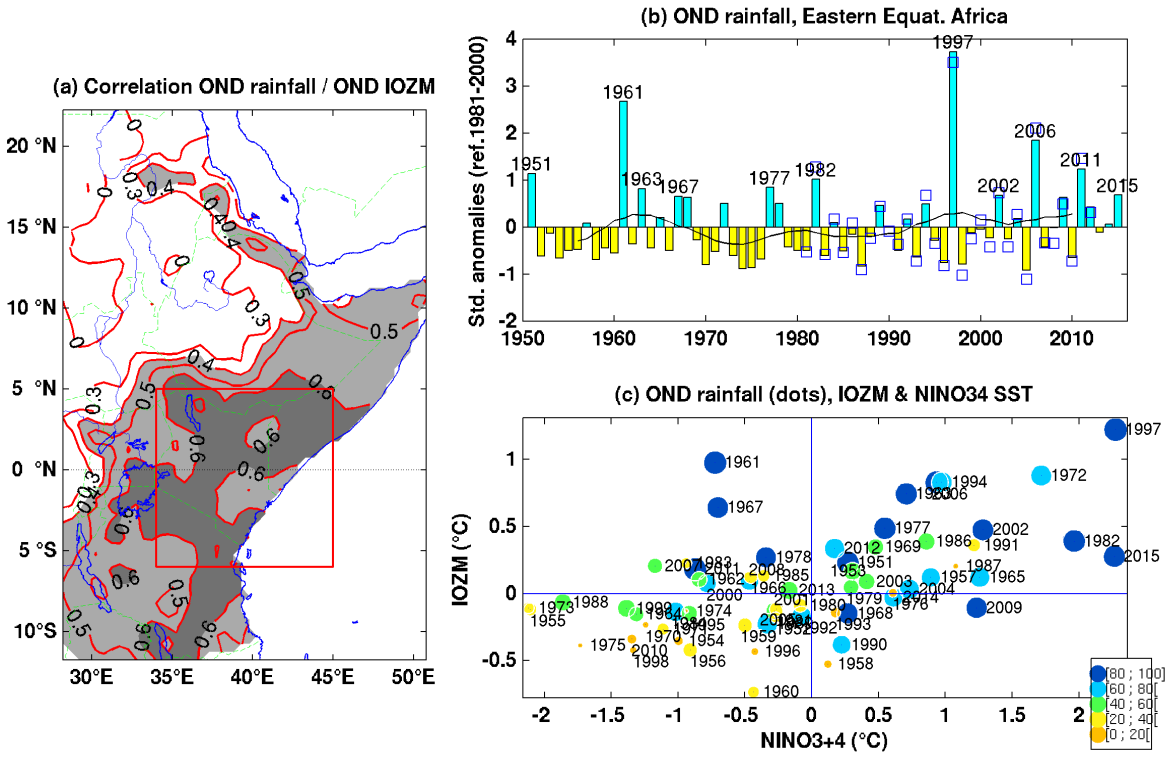

Fig.18 : Relationship between October-December rainfall and IOZM sea surface temperature. Rainfall data combined from CRC (1951-2012) and CHIRPS (2013-2015), both normalized on the period 1981-2000. (a) Correlation coefficients (1951-2015). Shading shows correlations above 0.4 (99.9% significance). (b) Time-series of standardized rainfall averaged for the Eastern Equatorial Africa index (red box in panel a). The smoothed line is a 11-yr moving average. Blue squares show the CHIRPS rainfall for 1981-2012. (c) Scatter-plot of OND values of the IOZM and Nino 3+4 SSTs. The color and size of the dots refer to quintiles of OND rainfall (e.g., dark blue : 20% wettest years ; orange : 20% driest years).

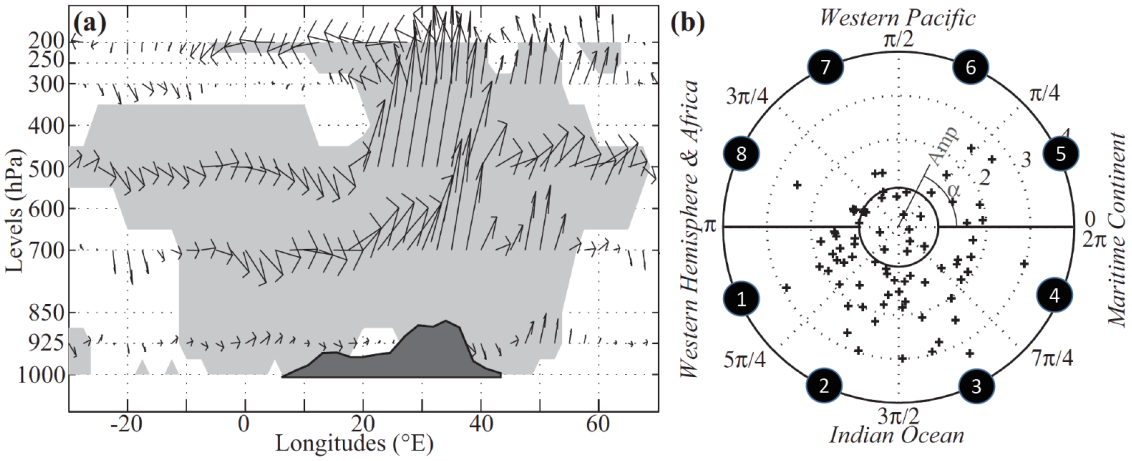

Fig.19 : Atmospheric dynamics and phases of the Madden-Julian Oscillation associated with heavy rainfall events in Western Kenya. (a) Vertical cross-section of the zonal wind and vertical motion along the equator (2.5 ◦ N–2.5 ◦ S) during the 5% wettest days of MAM 1979-1995 (after removal of the annual cycle). Significant anomalies are shaded (Hotelling t2-test, 95% level). (b) Distribution of the daily rainfall events (crosses) with respect to the MJO phase (circled numbers), α, and amplitude (radius). The location of the enhanced convective signal related to the MJO is shown against the main phases. The inner circle encompasses rainfall events occurring at times of weak MJO activity (amplitude <0.9) (reproduced from Pohl and Camberlin, 2006b).

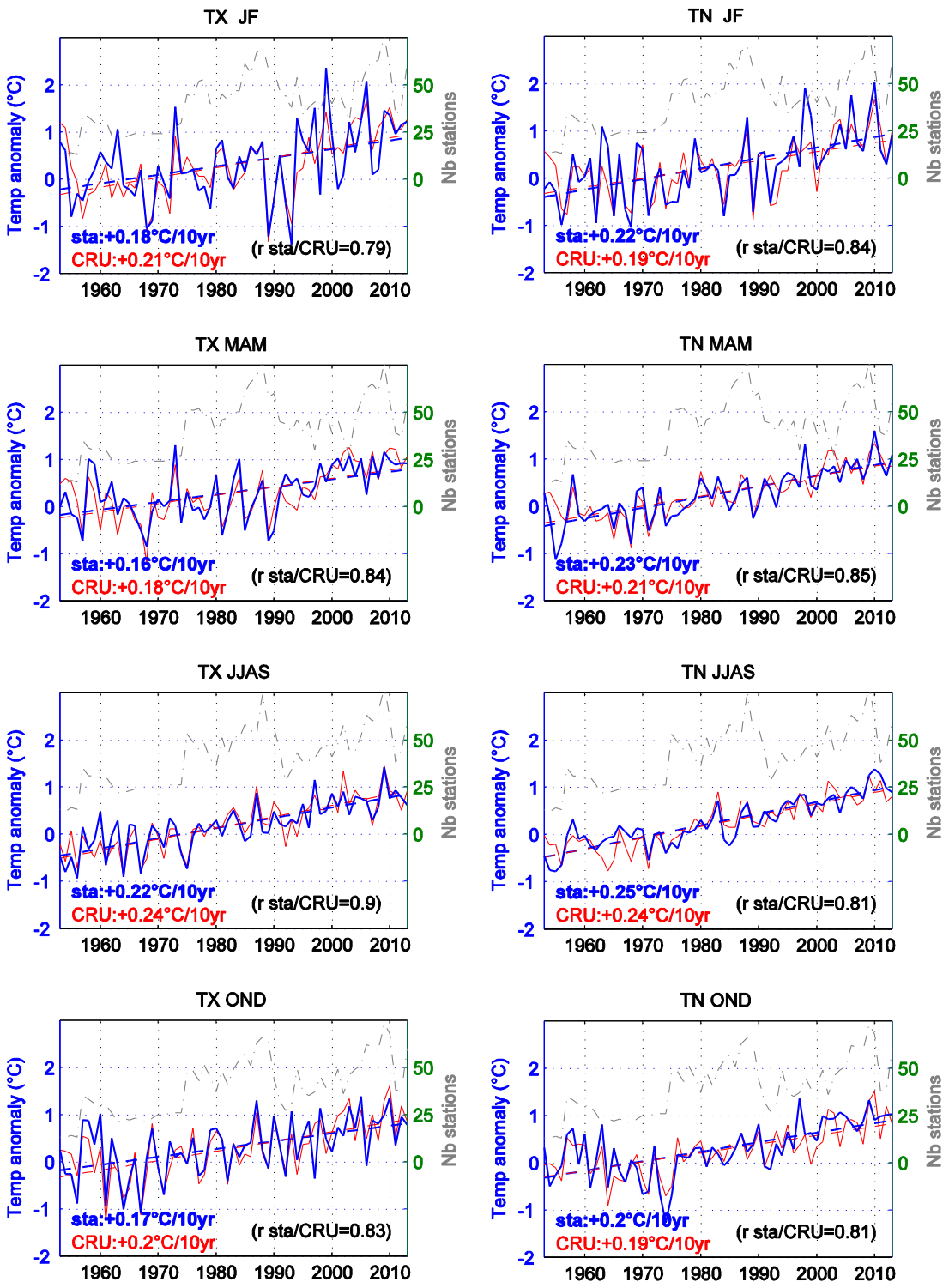

Fig.20 : Trends and interannual variations of seasonal mean maximum temperature (left panels) and minimum temperature (right panels), 1953-2013, for an index covering eastern Africa as a whole (Camberlin, 2016). Red thin lines : gridded CRU data. Blue thick lines : average temperature anomaly for available stations (number of stations : dash-dotted lines). The correlation coefficient between the station index and the CRU index is shown at bottom right corners. The station index is based on data from Global Historical Climate Network Daily (GHCND, Menne et al., 2012), Global Summary of the Day (GSOD) archived by NOAA and a few stations from the Kenya Meteorological Department. All station anomalies are computed with respect to the period 1961-1990, used as reference.

	Tx	Tn
CRC 98 stations	+1.16	+1.40
CRU grid-points with stations	+1.28	+1.28
Berkeley grid-points with stations	+1.10	+1.40
Berkeley all grid-points	+1.20	+1.45

Table 1 : Maximum (Tx) and minimum (Tn) temperature trends over Eastern Africa (1953-2013), in Celsius degrees over 61 years. CRC is an average of all available stations (98) as in fig.20. CRU and Berkeley Earth trends are computed as the spatial average over all grid-points containing at least one station in the CRC data set. The last line is the average of all grid-points within the region 12°S-23°N, 28-52°E for Berkeley Earth data (homogenized).